Cellular/Molecular

Rab6-Mediated Polarized Transport of Synaptic Vesicle Precursors Is Essential for the Establishment of Neuronal Polarity and Brain Formation

Yu Zhang,[1]* Masataka Kunii,[1]* Manabu Taniguchi,[2] Shin-ichiro Yoshimura,[1] and Akihiro Harada[1]
Departments of [1]Cell Biology and [2]Anatomy and Neuroscience, Graduate School of Medicine, Osaka University, Osaka 565-0871, Japan

Neurons are highly polarized cells that are composed of a single axon and multiple dendrites. Axon–dendrite polarity is essential for proper tissue formation and brain functions. Intracellular protein transport plays an important role in the establishment of neuronal polarity. However, the regulatory mechanism of polarized transport remains unclear. Here, we show that Rab6, a small GTPase that acts on the regulation of intracellular vesicular trafficking, plays key roles in neuronal polarization and brain development. Central nervous system-specific Rab6a/b double knock-out (Rab6 DKO) mice of both sexes exhibit severe dysplasia of the neocortex and the cerebellum. In the Rab6 DKO neocortex, impaired axonal extension of neurons results in hypoplasia of the intermediate zone. In vitro, deletion of Rab6a and Rab6b in cultured neurons from both sexes causes the abnormal accumulation of synaptic vesicle precursors (SVPs) adjacent to the Golgi apparatus, which leads to defects in axonal extension and the loss of axon–dendrite polarity. Moreover, Rab6 DKO causes significant expansion of lysosomes in the soma in neurons. Overall, our results reveal that Rab6-mediated polarized transport of SVPs is crucial for neuronal polarization and subsequent brain formation.

Key words: **cell polarity; Golgi apparatus; knock-out mouse; Rab6; synaptic vesicle**

Significance Statement

Elucidation of the regulatory mechanism underlying neuronal polarization is crucial to understanding neuron development and brain formation. Intracellular polarized transport plays an essential role in the establishment of axon–dendrite polarity. In this study, by using central nervous system-specific Rab6a/b double knock-out mice and primary cultured neurons, we showed the physiological role of Rab6 in neuronal polarization and subsequent neocortical IZ formation in vivo. Mechanistically, we revealed that Rab6 regulates the post-Golgi anterograde transport of synaptic vesicle precursors, which contributes to axonal extension in developing neurons.

Introduction

Neurons are highly polarized cells that are compartmentalized into two structurally and functionally distinct domains. They typically form a single long axon and multiple short dendrites during their differentiation. This axon–dendrite polarity is required for the formation of normal brain structures and neuronal networks; therefore, neuronal polarity is a fundamental property for neuronal activities that regulates higher brain functions, such as perception, memory, and behavior (Solecki et al., 2006; Arimura and Kaibuchi, 2007; Barnes and Polleux, 2009; Tahirovic and Bradke, 2009; Kon et al., 2017). In developing neurons, the generation of different compositions of proteins in each neurite is necessary for the specification of axons or dendrites. This process is strictly regulated by the machinery of directional intracellular transport of each protein, which is called polarized transport (Bradke and Dotti, 1997; Bentley and Banker, 2016; Guillaud et al., 2020; Radler et al., 2020).

Rab proteins are small GTPases that regulate divergent steps, such as vesicle biogenesis, maturation, transport, and targeting, in the intracellular transport of proteins and lipids (Zerial and McBride, 2001; Stenmark, 2009). Previous studies have shown that several Rab family members, such as Rab10, Rab27, and

Received Dec. 14, 2023; revised May 13, 2024; accepted May 26, 2024.
Author contributions: M.K. and A.H. designed research; Y.Z., M.T., S.Y., and A.H. performed research; Y.Z., M.K., and M.T. analyzed data; Y.Z., M.K., and A.H. wrote the paper.
We thank Dr. T. Sumi, J. Wu, and all other members of Harada Laboratory for their helpful comments. We also thank Drs. N. Inagaki and K. Baba for kindly providing antibodies. Generation of Rab6 DKO mice was supported by IEXAS, Faculty of Medicine, Osaka University. Histological and biochemical experiments were supported by the Center for Medical Research and Education, Graduate School of Medicine, Osaka University.
This study was supported by Japan Society for the Promotion of Science KAKENHI grant numbers 21H02658 to A.H. and 21K06734 to M.K. and by The Japan Spina Bifida & Hydrocephalus Research Foundation and Takeda Science Foundation to M.K. Y.Z. was supported by the China Scholarship Council.
*Y.Z. and M.K. contributed equally to this work.
The authors declare no competing financial interests.
Correspondence should be addressed to Akihiro Harada at aharada@acb.med.osaka-u.ac.jp.
https://doi.org/10.1523/JNEUROSCI.2334-23.2024

Rab33a, are involved in axon outgrowth and polarity establishment by regulating vesicular trafficking in primary neurons (Arimura et al., 2009; Wang et al., 2011; Nakazawa et al., 2012; Villarroel-Campos et al., 2016). However, the detailed mechanism of neuronal polarization through Rab-mediated polarized transport in vivo remains unclear.

Rab6 is an evolutionarily conserved Rab GTPase that is mainly localized on the trans-Golgi and trans-Golgi network (TGN). Murine Rab6 is composed of two paralogs: Rab6a and Rab6b. Rab6a has an alternative splicing variant, Rab6a′, which differs in only three amino acids (Echard et al., 2000). Rab6a and Rab6a′ (hereinafter referred to as Rab6a) are ubiquitously expressed and involved in the regulation of various anterograde and retrograde transport pathways from and to the Golgi apparatus (White et al., 1999; Mallard et al., 2002; Grigoriev et al., 2007; Miserey-Lenkei et al., 2017). Moreover, it has been suggested that Rab6b regulates vesicular trafficking in the nervous system because of its almost exclusive expression in the brain (Opdam et al., 2000; Wanschers et al., 2007; Nyitrai et al., 2020). Because Rab6a and Rab6b share >90% of their amino acids, their functional redundancy in the secretory pathway in neuronal or non-neuronal cells has also been suggested (Schlager et al., 2010, 2014; Homma et al., 2019). Recently, it has been reported that forebrain-specific Rab6a/b double knockout (Rab6 DKO) mice exhibited severe hypoplasia of the cerebral cortex (Brault et al., 2022). In this report, Rab6-mediated polarized apical transport of Crumbs3, a component of the apical junctional complex, in radial glial cells (RGCs) was critical for the prevention of RGC delamination (Brault et al., 2022). This report revealed the in vivo role of Rab6 in brain development through the regulation of polarized transport in RGCs; however, its function in mature neurons has not been identified.

Here, we show that Rab6 plays an essential role in the establishment of neuronal polarity, which contributes to the formation of the cerebral cortex. We generated central nervous system (CNS)-specific Rab6 DKO mice and observed severe hypoplasia of DKO brains, similar to the one in the recent report mentioned above. In addition to the abnormalities in RGCs, the neocortex of Rab6 DKO mice showed an extremely thin intermediate zone (IZ) caused by impaired axonal extension of newborn neurons. By using primary cultured neurons, we found the loss of neuronal polarity and the accumulation of synaptic vesicle precursors (SVPs) adjacent to the Golgi apparatus in Rab6 DKO neurons. Furthermore, we found the dysfunctional and abnormal enlarged lysosomes in the soma of Rab6 DKO neurons. Altogether, we conclude that Rab6 is crucial for the establishment of axon–dendrite polarity through the regulation of post-Golgi trafficking of SVPs toward axons in neurons.

Materials and Methods

Mice. All animal experiments were performed according to the guidelines of the Animal Care and Experimentation Committee of Osaka University. The animals were bred at the Institution of Experimental Animal Sciences, Faculty of Medicine, Osaka University (IEXAS).

The following transgenic lines of both sexes were used. *Rab6a*$^{flox/flox}$ mice were generated as previously described (Iwaki et al., 2020). To generate *Rab6b*$^{-/-}$ mice, a frameshift in the coding sequence was created by using CRISPR/Cas9 technology. An sgRNA sequence targeting the boundary region of *Rab6b* intron 1 and exon 2 (5′-CCTTGCAGT CGGGAAGACGTCTC-3′) was selected and inserted into the pX330 vector (#42230; Addgene). Fertilized eggs were injected with 80 ng/μl NLS-Cas9 mRNA, 50 ng/μl *Rab6b* sgRNA in 10 mM Tris-HCl and 0.1 mM EDTA in vitro as previously described (Yoshimi et al., 2014). Mutations in the *Rab6b* gene were analyzed by DNA sequencing. A 59 bp deletion in exon 2 resulted in a frameshift mutation, which encoded a truncated protein of only 28 amino acids.

To obtain *Rab6a*$^{flox/flox}$; *Rab6b*$^{-/-}$ mice, *Rab6a*$^{flox/flox}$ mice were crossed with *Rab6b*$^{-/-}$ mice. We then crossed these mice with *Nestin-Cre* transgenic mice (Tronche et al., 1999; The Jackson Laboratory) to generate *Nestin-Cre*; *Rab6a*$^{flox/flox}$; *Rab6b*$^{+/-}$ mice. *Nestin-Cre*; *Rab6a*$^{flox/flox}$; *Rab6b*$^{+/-}$ mice were crossed with *Rab6a*$^{flox/flox}$; *Rab6b*$^{-/-}$ mice to obtain Rab6a/b double knock-out mice (*Nestin-Cre*; *Rab6a*$^{flox/flox}$; *Rab6b*$^{-/-}$, abbreviated Rab6 DKO). Genomic PCR was used to determine the genotypes by using the following primers: F: 5′-ACGTATAGCCGAAATTGCCAGGATC-3′ and R: 5′-ATCTCCGG TATTGAAACTCCAGCGC-3′ for the *Cre* transgenic allele; F: 5′-G CCATTCTTACTGGGGAACATTAAGATACTC-3′ and R: 5′-CATG CACTAAGCACACACTCTGTGTTGGAG-3′ for the *Rab6a* floxed allele; and F: 5′-GAATTCCGATGAGTGGTCAGGTGGTCTATCCAG-3′ and R: 5′-GAATTCGTAAGTTGCCTGAGAGAGCTGCAGTGG-3′ for the *Rab6b* allele.

Antibodies. The following primary and secondary antibodies were used in this study: anti-Rab6a (rabbit; Cell Signaling Technology, D37C7), anti-Rab6a (mouse; Sigma-Aldrich, H7171-3G3), anti-Rab6b (rat; Abcam, ab95374), anti-GAPDH (mouse; Calbiochem, CB1001), anti-Pax6 (rabbit; Covance, PRB-278P), anti-Tbr2 (rabbit; Abcam, ab23345), anti-cleaved caspase-3 (rabbit; Cell Signaling Technology, 9661), anti-Tbr1 (rabbit; Millipore, AB10554), anti-Cux1 (rabbit; Santa Cruz Biotechnology, sc-13024), anti-pMAP1B (mouse; Sato-Yoshitake et al., 1989), anti-Tuj1 (mouse; Covance, MMS-435P), anti-GM130 (mouse; BD Biosciences, 610822), anti-β-actin (mouse; Sigma-Aldrich, A5441), anti-shootin1 (rabbit; a kind gift from Dr. Naoyuki Inagaki, Nara Institute of Science and Technology, Japan), anti-IGF1R (rabbit; Cell Signaling Technology, D23H3), anti-CHGB (mouse; Atlas Antibodies, AMAb91709), anti-synaptotagmin 1 (mouse; Developmental Studies Hybridoma Bank, AB2199314), anti-Golgin97 (rabbit; Cell Signaling Technology, D8P2K), anti-synaptophysin 1 (mouse; Progen, 61012), anti-PIST (mouse; Santa Cruz Biotechnology, sc-393026), anti-Tom20 (mouse; Santa Cruz Biotechnology, sc-17764), anti-KIF1A (rabbit; Abcam, ab180153), anti-Rab33a (mouse; Proteintech, 68389-1-Ig), anti-TrkB (mouse; BD Biosciences, 610101), anti-EEA1 (goat; Santa Cruz Biotechnology, sc-6415), FITC-conjugated anti-CD71 (rat; BioLegend, 113805), anti-LAMP1 (rat; eBioscience, 14-1071), anti-LAMP2 (rat; Developmental Studies Hybridoma Bank, ABL-93), anti-Cathepsin D (goat; R&D Systems, AF1029), Alexa Fluor 488-, Alexa Fluor 568-, and Cy5-labeled donkey anti-rabbit, anti-rat, anti-mouse, and anti-goat IgG (Molecular Probes), and HRP-labeled donkey anti-mouse and anti-rat IgG (Jackson ImmunoResearch Laboratories). Nuclei were stained with 4′,6-diamidino-2-phenylindole (DAPI). Rhodamine-phalloidin (Invitrogen, R415) was used to visualize cell shape.

Histological analysis. Embryonic day 18.5 (E18.5) embryos of both sexes were used for histological analysis. Most of the procedures used were performed as previously described (Kunii et al., 2021). For hematoxylin and eosin (H&E) staining, they were intracardially perfused with 3% paraformaldehyde in 0.1 M phosphate buffer, pH 7.4. The heads were immersed in the same fixative at 4°C overnight for additional fixation. To protect the abnormal morphology of Rab6 DKO brains, the skull bones were not completely removed. After fixation, the heads were decalcified in decalcification solution (10% EDTA, 1.2% Tris, pH 7.4) for 3 d at 4°C. After decalcification, the heads were dehydrated in ethanol and embedded in paraffin. The paraffin blocks were cut into 4 μm sections using a microtome (RM2145, Leica). The paraffin-embedded brain sections were stained with H&E solution. For immunofluorescence staining, embryonic brains were consecutively immersed in 10 and 20% sucrose in 0.1 M phosphate buffer, pH 7.4, for cryoprotection after perfusion. The brains were then embedded in O.C.T. Compound (Sakura Finetek) and rapidly frozen in liquid nitrogen. The frozen blocks were cut into 14 μm sections using a cryostat (CM3050S, Leica). The sections were blocked with blocking buffer (5% normal donkey serum and 0.1%

saponin in PBS) for 5 min and subsequently incubated with the appropriate primary antibodies and secondary antibodies in blocking buffer. Nuclei were stained with DAPI. The stained sections were mounted with Mowiol mounting medium. Confocal images were obtained using a laser scanning confocal microscope (FV1000D, Olympus) with UPLSAPO 10×, 20×, and 40× objective lenses (NA 0.40, 0.75, and 1.25, respectively, Olympus).

Immunoblotting. E18.5 embryonic brains or primary neurons from both sexes were lysed in SDS-PAGE sample buffer [63 mM Tris-HCl, pH 6.8, 10% (v/v) glycerol, 3% SDS, 0.05% bromophenol blue, and 3.3% (v/v) 2-mercaptoethanol], followed by sonication and heating at 95°C for 5 min. The concentration of the protein samples was measured using the XL-Bradford kit (APRO Science Group). SDS-PAGE and immunoblotting were performed as previously described (Kunii et al., 2021). The immunoreactive bands were detected using Immobilon Western HRP substrate (Millipore) and a ChemiDoc Touch imaging system (Bio-Rad).

Culture of primary cortical neurons. Cortical neurons were dissociated and cultured as previously described (Teoh et al., 2017). In brief, the neocortex was dissected from E17.5 embryos of both sexes of two genotypes (*Rab6a*$^{flox/flox}$; *Rab6b*$^{+/+}$ and *Rab6a*$^{flox/flox}$; *Rab6b*$^{-/-}$), incubated with dissociation solution (0.5 mg/ml papain, 1 mg/ml BSA, 12 μg/ml DNase, and 1.8 mg/ml glucose in PBS) for 20 min at 37°C and dissociated by gentle trituration. The isolated neurons were cultured in plating medium [10% FBS (Corning) and GlutaMAX (Invitrogen) in Neurobasal medium (Invitrogen)] and plated on 35 mm glass bottom dishes (Matsunami) or 35 mm plastic dishes (Corning) coated with poly-D-lysine (Sigma-Aldrich) and laminin (Corning). The plating medium was replaced with complete medium [Neurobasal medium supplemented with B27 (Invitrogen) and GlutaMAX] after 2 h. The cultures were maintained at 37°C and 5% CO_2 in a humidified incubator until experiments. To knock-out Rab6a, a Cre recombinase-expressing adenovirus was added to the complete medium as previously described (Avriyanti et al., 2015). Neurons infected with a LacZ-expressing adenovirus were used as controls. The medium was replaced with virus-free complete medium after 24 h.

For the immunostaining of neurons, the cells were fixed with 3% paraformaldehyde in 0.1 M phosphate buffer, pH 7.4, for 15 min at room temperature (RT), blocked with blocking buffer for 5 min, immunostained with appropriate antibodies and rhodamine-phalloidin (Invitrogen, R415), and mounted with Mowiol mounting medium. Images were obtained using a laser scanning confocal microscope (LSM880, Zeiss) equipped with an Airyscan detector and Plan-Apochromat 25× and 63× objective lenses (NA 0.8 and 1.4, respectively, Zeiss). The images were then processed by Airyscan image processing using ZEN software.

For immunoelectron microscopy, DIV3 neurons were fixed with periodate-lysine-paraformaldehyde fixative (10 mM $NaIO_4$, 75 mM lysine, 4% PFA in 37.5 mM phosphate buffer, pH 7.2) for 2 h at RT. After fixation, the neurons were blocked and permeabilized in blocking solution (5% normal goat serum and 0.25% saponin in PBS) for 15 min at RT. They were then incubated with synaptophysin antibody in blocking solution for 1 h at 37°C. After washed with PBS for three times, the neurons were incubated with secondary antibody (goat anti-mouse Alexa Fluor 488-labeled FluoroNanogold; #7202, Nanoprobes) in blocking buffer for 1 h at RT. The samples were then silver enhanced with HQ silver enhancement solution (#2012, Nanoprobes) for 7 min at RT and incubated with 5% selenium toner (Kodak) for 7 min at RT. The samples were postfixed with 2.5% glutaraldehyde in HEPES buffer (30 mM HEPES, 100 mM NaCl, 2 mM $CaCl_2$, pH 7.4) at RT overnight. On the next day, the samples were washed with HEPES buffer and postfixed with 1% osmium tetroxide and 1.5% potassium ferrocyanide in HEPES buffer for 45 min on ice. The fixed neurons were then stained with 0.5% uranyl acetate in distilled water for overnight. After these steps, the samples were dehydrated and embedded in Quetol-812 (Nisshin EM). The cells were cut into ultrathin sections using an ultramicrotome (Reichert Ultracut N). Electron micrographs were obtained using a transmission electron microscope (HT7800, HITACHI).

Measurement of neurite length and analysis of neuronal morphology. Cultured cortical neurons were fixed at 24, 48, and 72 h after adenovirus addition. The cells were immunostained with Tuj1 antibody to visualize neurites. In the stained dishes, areas 185 μm × 185 μm in size were selected randomly and photographed using an LSM880 microscope (Zeiss) with a 25× objective lens (NA 0.8, Zeiss). The length of each soma-derived neurite and the number of soma-derived neurites were measured using the NeuronJ plugin (Meijering et al., 2004) in ImageJ (National Institutes of Health). A neurite was considered to be an axon if the length of the neurite was more than twice the length of any other neurite and the diameter of the cell body (Yin et al., 2008). The cells were categorized into different developmental stages according to the following criteria (Tahirovic and Bradke, 2009): cells with a round shape bearing lamellipodia were considered Stage I neurons; cells with multiple neurites of similar length were regarded as Stage II neurons; and cells with an axon and several minor neurites were determined to be Stage III neurons.

Retention using selective hooks (RUSH) assay. A coding sequence of synaptotagmin1 (Syt1) was amplified from the mouse brain cDNA library (Clontech) by PCR. E-cadherin cDNA in Str-KDEL_SBP-EGFP-E-cadherin RUSH plasmid (kind gifts from Dr. Franc Perez) was replaced with Syt1 cDNA using FseI and XhoI.

Cortical neurons were plated on 35 mm glass bottom dishes and transfected at DIV 2 using Lipofectamine LTX Reagent (15338, Invitrogen). Neurons were first washed twice with the Neurobasal medium. The transfection mixture (2 μg plasmid DNA, 2 μl Lipofectamine LTX reagent, and 2 μl Plus reagent in 400 μl Opti-MEM) was then added into the medium. The neurons were incubated at 37°C and 5% CO_2 in a humidified incubator for 1 h. After that, neurons were washed with Neurobasal medium once and incubated with the complete medium overnight until being assayed.

To induce the trafficking from the ER, the medium was added with biotin at a final concentration of 40 μM. The neurons were then fixed at 0, 15, 30, 45, 60, and 120 min after biotin treatment, respectively, and stained with Golgin97 or LAMP2 antibodies.

Protein production and purification from Escherichia coli. The protein production procedures were described previously (Nakajo et al., 2016). Hexahistidine-GST tagged Rab6aQ72L, Rab6bQ72L, or Rab6bT27N were expressed in Rosetta 2 (DE3) pLysS cells (Novagen) using the pFAT2 vector. The cells were cultured in 4 L of LB medium containing 100 μg/ml ampicillin, 34 μg/ml chloramphenicol, and 0.25 mM IPTG at 18°C for 17 h. The bacterial pellets were harvested by centrifugation, resuspended with IMAC20 (20 mM Tris-HCl, pH 8.0, 300 mM NaCl, and 20 mM imidazole), and sonicated on ice. The supernatant was collected after centrifugation and incubated with 1 ml of Ni-NTA Agarose (Qiagen) at 4°C for 2 h. The beads were washed three times using IMAC20 containing 1 mM ATP and 1 mM $MgCl_2$. The bound protein was eluted with IMAC200 (20 mM Tris-HCl, pH 8.0, 300 mM NaCl, and 200 mM imidazole) and dialyzed in PBS for overnight at 4°C. The aliquots were stored at −80°C after snap-frozen.

GST pull-down assay and mass spectrometry. For the GST pull-down assay, 500 μg of GST-Rab6aQ72L, GST-Rab6bQ72L, or GST-Rab6bT27N proteins expressed in *E. coli* were bound to 50 μl of Glutathione Sepharose 4B (GE Healthcare) in a 10 ml total volume of NL100 (20 mM HEPES-NaOH, pH 7.5, 100 mM NaCl, 5 mM $MgCl_2$, 0.1% Triton X-100) for 1 h at 4°C. The beads were washed three times with NL100 and incubated with a 9 ml total volume of 25 mg mouse brain lysate freshly prepared in precooled NL100 containing 1% protease inhibitor cocktail and 5 mM GTP (for QL mutant) or GDP (for TN mutant) for 1 h at 4°C. The beads were washed three times with NL100 and then once with NL200 (20 mM HEPES-NaOH, pH 7.5, 200 mM NaCl, 5 mM $MgCl_2$, 0.1% Triton X-100). The bound proteins were subsequently eluted with 500 μl of NE500 (20 mM HEPES-NaOH, pH 7.5, 500 mM NaCl, 20 mM EDTA, 0.1% Triton X-100). The eluted proteins were precipitated using 10 μl of 1% deoxycholic acid and 60 μl of TCA for 30 min on ice and washed twice with

ice-cold acetone. The precipitated proteins were dissolved in 40 µl of SDS–PAGE sample buffer.

For the mass spectrometry, 10 µl of the protein samples were separated on a NuPAGE 4–12% Bis-Tris Gel (Thermo Fisher Scientific) and silver stained using a silver stain mass spectrometry kit (Wako) according to the manufacturer's instructions. The lanes were cut from the gel, and the proteins were reduced, alkylated, and digested with trypsin. The samples were analyzed using a SYNAPT G2 mass spectrometer (Waters) at Osaka University Center for Medical Research and Education. The database search was conducted using ProteinLynx Global Server software, version 2.4 (Waters) and the International Protein Index database (mouse; v.3.77).

Proximity ligation assay. The proximity ligation assay (PLA) was performed using the Duolink In Situ Detection Reagents Red (DUO92008, Sigma). In brief, DIV3 neurons were fixed with 3% PFA and then permeabilized with 0.1% saponin. The neurons were then blocked with Duolink blocking buffer, incubated with indicated primary antibodies for 1 h at 37°C, and incubated with PLA probe anti-rabbit MINUS (DUO92005, Sigma) and PLA probe anti-mouse PLUS (DUO92001, Sigma) at 37°C for 1 h, sequentially. After these steps, the neurons were treated with ligation solution and amplification solution according to the manufacturer's protocol. Nuclei were stained with DAPI. Images were obtained using a laser scanning confocal microscope (LSM880, Zeiss) equipped with an Airyscan detector and Plan-Apochromat 63× objective lenses (NA 1.4, Zeiss). The images were then processed by Airyscan image processing using ZEN software.

Assessment of the lysosomal pH. The lysosomal pH was assessed using the Lysosomal Acidic pH Detection Kit (#L266; Dojindo Laboratories), according to the manufacturer's instructions. Briefly, DIV3 neurons were cultured in 35 mm glass bottom dishes and stained with LysoPrime Green and pHLys Red for 30 min at 37°C, sequentially. Fluorescence images of live neurons were obtained using a laser scanning confocal microscope (LSM880, Zeiss) equipped with an Airyscan detector and Plan-Apochromat 63× objective lenses (NA 1.4, Zeiss).

Experimental design and statistical analysis. For all experiments, the control and experimental genotypes were tested at the same time at least three times.

Statistical analyses and data plotting were performed using GraphPad Prism software, version 9.5.0 (Dotmatics). Significance was calculated using Student's *t* tests or one-way analysis of variance (ANOVA). The results are presented as the mean ± SD. The *p* values are depicted as follows: $p < 0.05$ was considered significantly different (*, $p < 0.05$; **, $p < 0.01$; ***, $p < 0.001$; ****, $p < 0.0001$; ns represents not significant).

Results

Rab6 DKO mice exhibit severe dysplasia of the cerebral cortex and the cerebellum

In the developing mammalian brain, neurons are generated from neural progenitor cells (NPCs), such as RGCs and intermediate progenitor cells (IPCs), and migrate to precise positions to form neuronal layers (Greig et al., 2013; Butts et al., 2014; Fig. 1*A*). Immunofluorescence analysis showed that Rab6a and Rab6b exhibited similar expression patterns in the neocortex in wild-type mice at E18.5. These proteins are expressed in both NPCs in the ventricular zone (VZ) and the subventricular zone (SVZ) and newborn neurons in the cortical plate (CP; Fig. 1*B*). Their localizations are enriched in the soma in both NPCs and neurons, the ventricular surface of RGCs, and the IZ, which is composed of axons from neurons in the CP, suggesting that these two similar proteins might play key roles in both NPCs and neurons (Fig. 1*B*). To elucidate the in vivo functions of Rab6a and Rab6b in brain development, single KO mice were generated. Because conventional Rab6a KO in mice is embryonic lethal (Shafaq-Zadah et al., 2016), we generated CNS-specific Rab6a conditional KO (Rab6a cKO) mice by crossing *Rab6a*$^{flox/flox}$ mice with Nestin-Cre mice, resulting in Cre-mediated recombination in RGCs (Tronche et al., 1999; Iwaki et al., 2020). Rab6a cKO mice were born normally and showed no overt phenotype associated with brain morphogenesis (Fig. 1*D*). To knock out Rab6b, which is expressed almost exclusively in the brain (Opdam et al., 2000), we used a CRISPR/Cas9 technique to generate conventional KO mice. Rab6b KO mice were also born at the expected Mendelian ratio and showed normal brain morphology similar to that of control and Rab6a cKO mice (Fig. 1*D*). These results suggest their functional redundancy in brain development. Therefore, we generated CNS-specific Rab6a/b double KO (Rab6 DKO) mice. Rab6 DKO mice were born at the Mendelian ratio but died soon after birth; therefore, we used E18.5 embryos for the following analysis. Immunostaining and immunoblotting showed that Rab6a and Rab6b were deficient in the Rab6 DKO brain (Fig. 1*B*,*C*). H&E staining of sagittal sections of the whole brain showed that Rab6 DKO brains exhibited not only drastically reduced thickness of the cerebral cortex but also an obviously smaller cerebellum (Fig. 1*D*). In addition, the lateral ventricles and fourth ventricles of Rab6 DKO brains were correspondingly enlarged (Fig. 1*D*). This result suggested that Rab6a and Rab6b are essential in the normal development of the cerebral cortex and the cerebellum.

The Rab6 DKO neocortex exhibits impaired IZ formation

Recently, it has been reported that RGC delamination and increased cell death caused by impaired apical transport of Crumbs3, which is a component of the apical junctional complex in RGCs, leads to severe malformation of the neocortex in forebrain-specific Rab6 DKO mice (Brault et al., 2022). Our Rab6 DKO mice also showed reduced numbers of RGCs and IPCs, which were labeled by Pax6 and Tbr2, respectively, in the VZ/SVZ and an increased tendency to localize to the CP region of the neocortex (Fig. 2*A*–*E*). Additionally, the number of apoptotic cells labeled with cleaved Caspase-3 (CC3) was increased in the Rab6 DKO neocortex (Fig. 2*F*,*G*). Thus, in accordance with the recent report (Brault et al., 2022), our results suggested that ectopic localization of NPCs and increased cell death lead to dysplasia of the neocortex in Rab6 DKO mice.

The immunostaining results showed that Rab6a and Rab6b were also expressed in cortical neurons (Fig. 1*B*). We therefore hypothesized that dysplasia of the neocortex might be caused by abnormalities in neurons. To confirm this hypothesis, we analyzed the distribution of newborn neurons in the neocortex by immunostaining. In the developing neocortex, newborn neurons migrate radially and exhibit a birth date-dependent "inside-out" pattern. Early-born neurons, which are positive for Tbr1, are located in the deep layers of the CP, whereas late-born neurons, which are positive for Cux1, migrate past early-born neurons to the superficial layers (Greig et al., 2013; Figs. 1*A*, 2*A*). In the neocortex of all four genotypes, Tbr1-positive early-born neurons localized to the lower half of the CP, while Cux1-positive late-born neurons were located just beneath the marginal zone (MZ; Fig. 3*A*,*B*). These results suggested that the inside-out migration of newborn neurons was not influenced by the deletion of Rab6a/b. In the Rab6 DKO neocortex, however, both types of neurons were located in a lower region than those in the control neocortex (Fig. 3*A*–*D*). Because both Rab6a and Rab6b were enriched in axons in the IZ of the wild-type neocortex (Fig. 1*B*), we hypothesized that IZ formation by the extension of axons might be altered in the Rab6 DKO neocortex. To compare IZ formation, we stained the neocortex of each mouse with

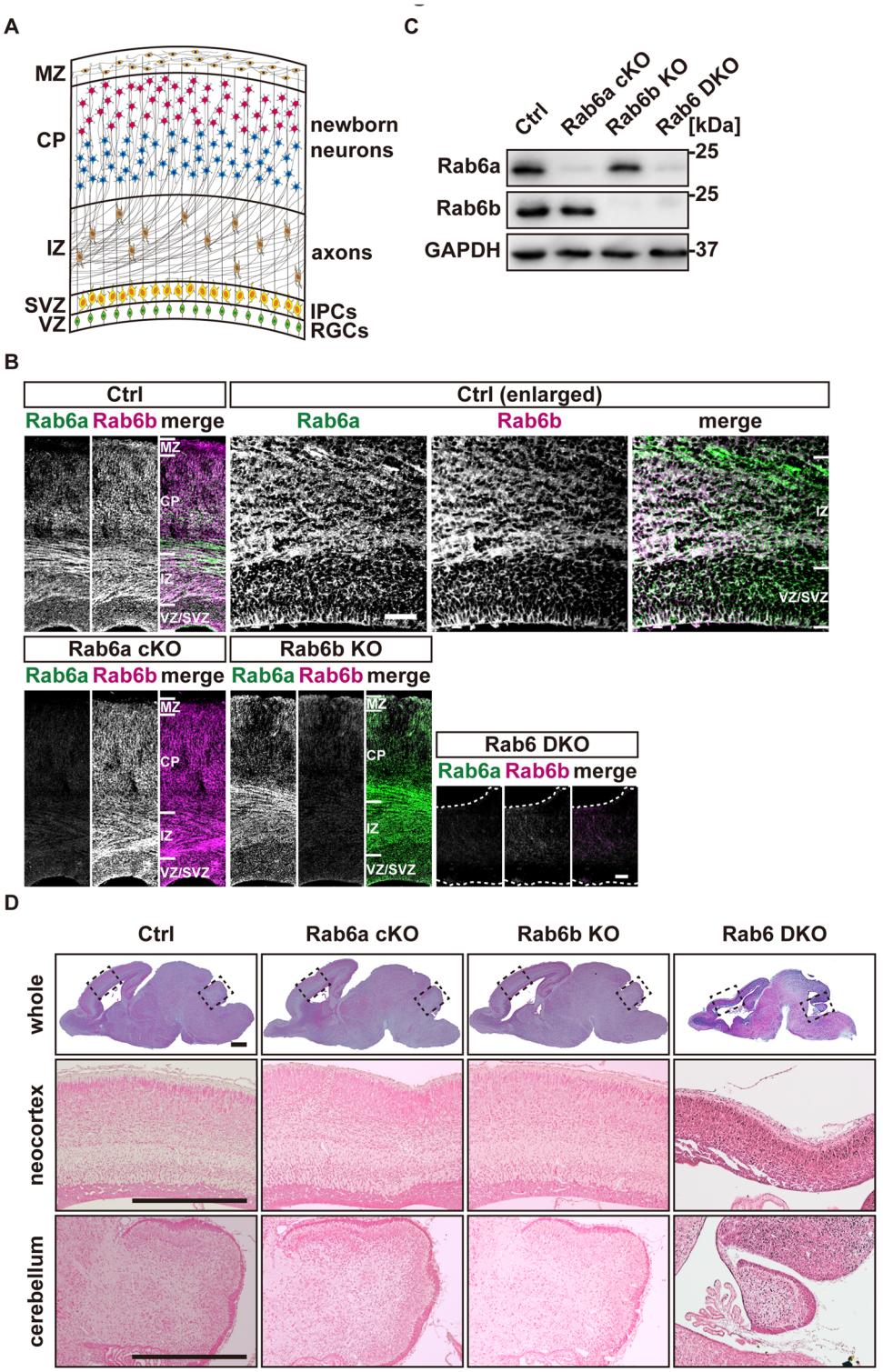

Figure 1. Rab6 DKO mice exhibit severe dysplasia of the cerebral cortex and the cerebellum. ***A***, Schematic illustration of the laminar organization of the E18.5 neocortex, showing the location of RGCs, IPCs, axons, and newborn neurons. VZ, ventricular zone; SVZ, subventricular zone; IZ, intermediate zone; CP, cortical plate; MZ, marginal zone; RGC, radial glial cell; IPC, intermediate progenitor cell. ***B***, Representative images showing the expression of Rab6a and Rab6b in E18.5 cerebral cortices of the indicated genotypes. The area between the two white dashed lines indicates the Rab6 DKO neocortex. Scale bars, 50 µm. ***C***, Western blot analysis of Rab6a and Rab6b expression in the E18.5 brains of the indicated genotypes. GAPDH was used as a loading control. ***D***, Representative images of H&E staining of E18.5 sagittal brain sections of the indicated genotypes. The bottom panels show magnified images of the boxes surrounded by dashed lines in the top panels. Scale bars, 500 µm.

phosphorylated-MAP1B (pMAP1B) antibody. MAP1B is a microtubule-associated protein that is specifically expressed during neuronal development. The phosphorylated form of MAP1B is mainly present in developing axons (Boyne et al., 1995). In the control neocortex, as well as Rab6a cKO and Rab6b KO, pMAP1B-positive axon bundles formed the IZ between the SVZ and the CP (Fig. 3*E*). Conversely, the Rab6 DKO neocortex exhibited severely thinner pMAP1B-positive bundles, which

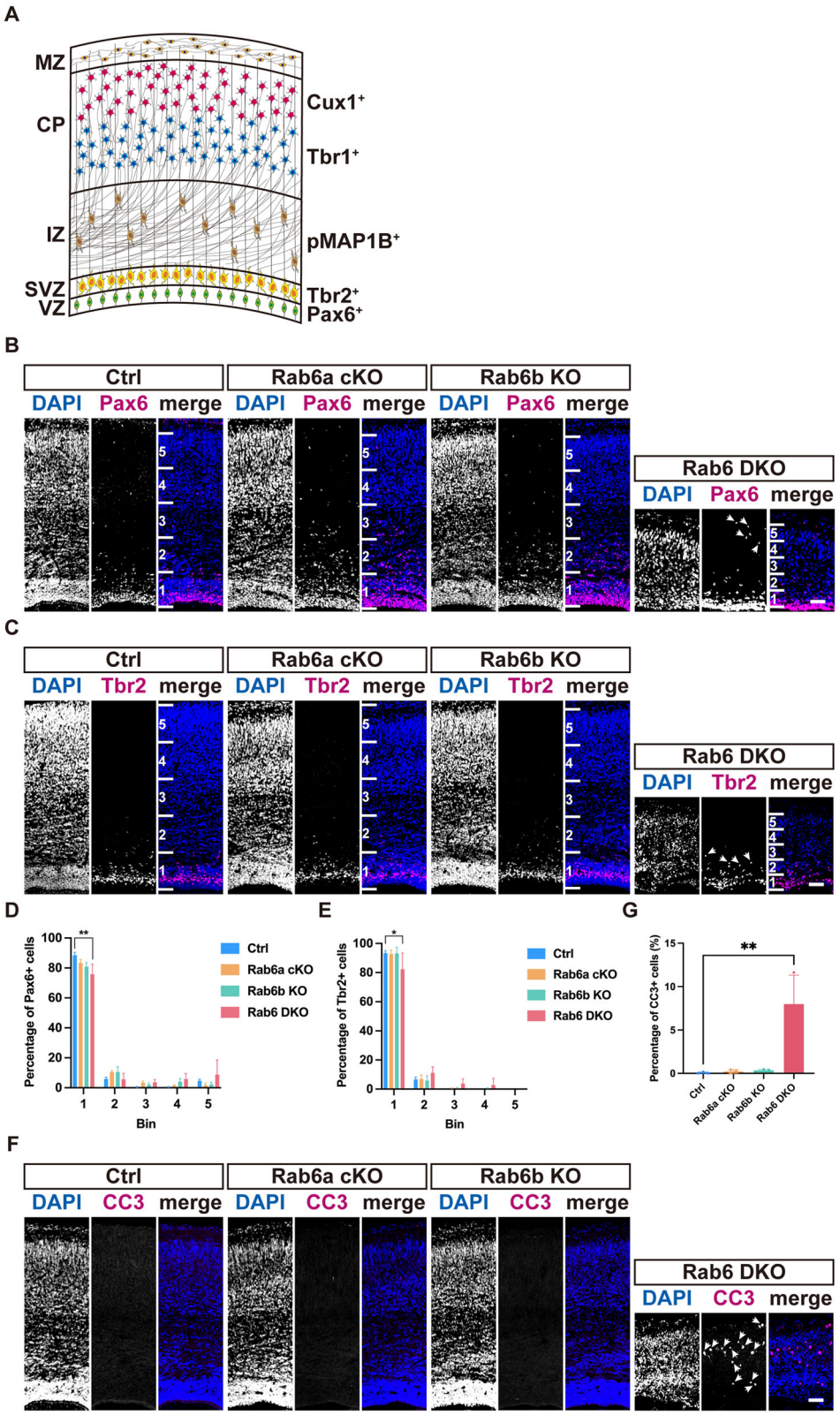

Figure 2. Rab6 DKO causes ectopic NPCs. ***A***, Schematic illustration of the laminar organization of the E18.5 neocortex, showing the expression domains for Pax6-positive (green), Tbr2-positive (yellow), Tbr1-positive (blue), and Cux1-positive (red) cells. VZ, ventricular zone; SVZ, subventricular zone; IZ, intermediate zone; CP, cortical plate; MZ, marginal zone. ***B***, ***C***, Representative images of Pax6 (magenta in ***B***) or Tbr2 (magenta in ***C***) staining in coronal sections of E18.5 cortices of the indicated genotypes. Nuclei were stained with DAPI (blue). Arrows in Rab6 DKO panels indicate ectopic NPCs. Scale bars, 50 µm. ***D***, ***E***, Quantification of the distribution of Pax6-positive (***D***) or Tbr2-positive (***E***) cells in E18.5 cerebral cortices ($n = 3$ sections from 3 brains per genotype, $^{**}p = 0.0039$, $^{*}p = 0.0252$, one-way ANOVA with Tukey's multiple-comparisons test). ***F***, Representative images of cleaved caspase 3 (CC3) (magenta) staining in coronal sections of E18.5 cortices of the indicated genotypes. Nuclei were stained with DAPI (blue). Arrows in Rab6 DKO panels indicate CC3-positive cells. Scale bar, 50 µm. ***G***, Quantification of the percentage of CC3 positive cells in E18.5 cerebral cortices ($n = 3$ sections from 3 brains per genotype, $^{**}p = 0.0018$, one-way ANOVA with Tukey's multiple-comparisons test). Values are represented as the mean ± SD. $^{*}p < 0.05$; $^{**}p < 0.01$. Ctrl, control.

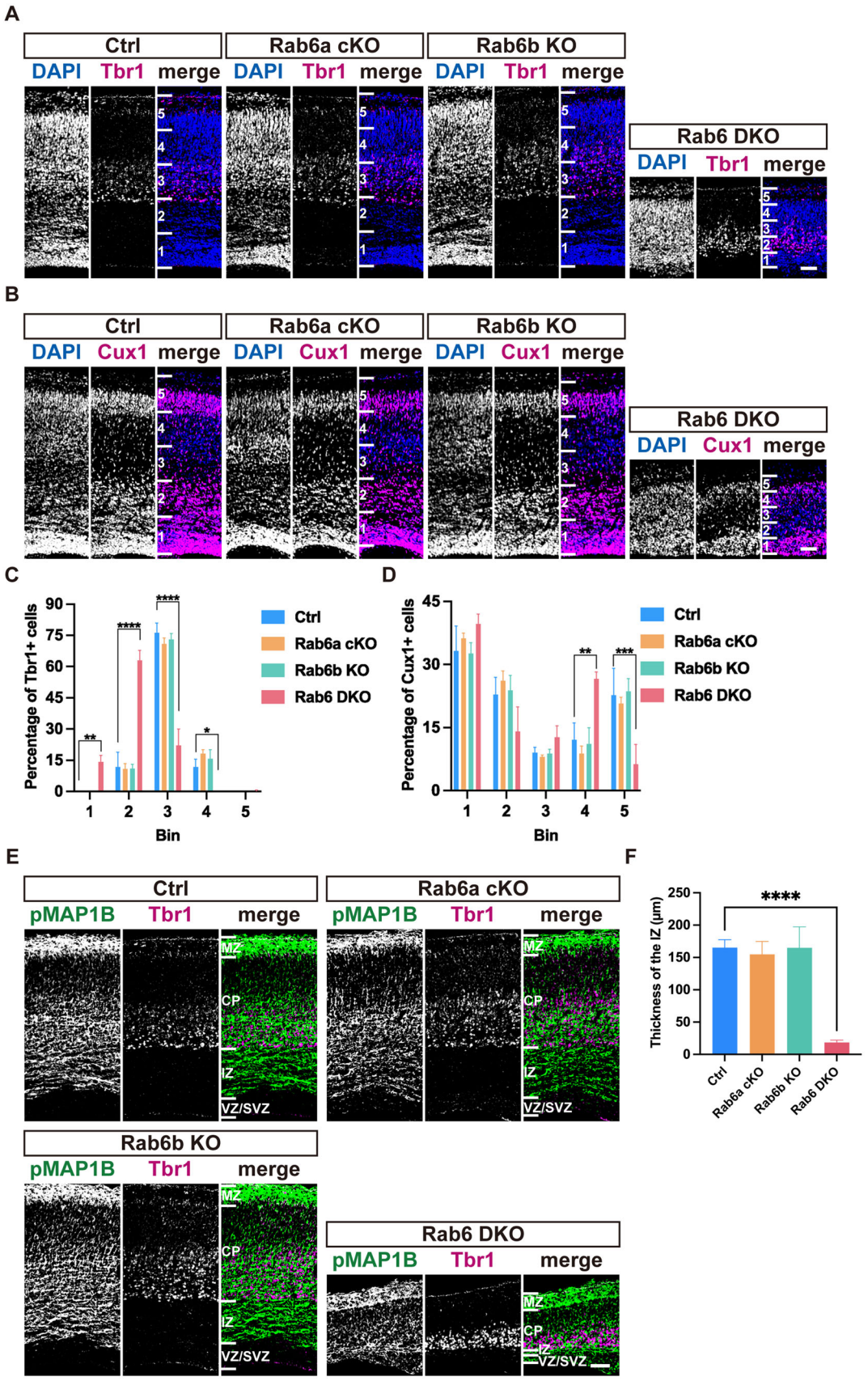

Figure 3. The Rab6 DKO neocortex exhibits impaired IZ formation. ***A***, ***B***, Representative images of Tbr1 (magenta in ***A***) or Cux1 (magenta in ***B***) staining in coronal sections of E18.5 cortices of the indicated genotypes. Nuclei were stained with DAPI (blue). Scale bars, 50 μm. ***C***, Quantification of the distribution of Tbr1-positive neurons in E18.5 cerebral cortices ($n = 3$ sections from 3 brains per genotype, $^{**}p = 0.0012$ Bin 1, $^{****}p < 0.0001$ Bin 2, $^{****}p < 0.0001$ Bin 3, $^{*}p = 0.014$ Bin 4, one-way ANOVA with Tukey's multiple comparison test). ***D***, Quantification of the distribution of Cux1-positive neurons in E18.5 cerebral cortices ($n = 3$ sections from 3 brains per genotype, $^{**}p = 0.0011$ Bin 4, $^{***}p = 0.0001$ Bin 5, one-way

indicated a defect in IZ formation caused by a decrease in axonal extension (Fig. 3*E*,*F*). Overall, we conclude that impaired IZ formation is responsible for hypoplasia of the Rab6 DKO cerebral cortex.

Rab6 DKO results in decreased axonal extension

To assess the defect in axonal extension during neuronal development, we cultured primary neurons from E17.5 embryonic cortices. At 72 h, almost all the control neurons, which were labeled by βIII tubulin (Tuj1) antibody, were classified as Stage III neurons in vitro (Tahirovic and Bradke, 2009), and these neurons had one single long axon and a few short dendrites (Fig. 4*A*, top left). Rab6a and Rab6b were detected as punctate signals in both the soma and neurites; however, their localization was slightly different from each other. Namely, Rab6a accumulated more in the perinuclear region (Fig. 4*A*,*B*, arrows), whereas Rab6b was more dispersed in the soma and distributed to the distal axon, in addition to perinuclear localization (Fig. 4*A*, arrowheads in the bottom left panel). This axonal localization of Rab6b might suggest a specific role of Rab6b in capturing transport vesicles in presynaptic boutons, as reported previously (Nyitrai et al., 2020). The accumulation of Rab6a and Rab6b in the perinuclear region partially colocalized with GM130, a Golgin protein localized at the cis-Golgi, indicating their Golgi localization (Fig. 4*B*, top panels).

To obtain Rab6a KO, Rab6b KO, and Rab6 DKO neurons, primary neurons from *Rab6a*$^{flox/flox}$; *Rab6b*$^{+/+}$ and *Rab6a*$^{flox/flox}$; *Rab6b*$^{-/-}$ cortices were infected with adenoviruses expressing LacZ (Ad-LacZ) or Cre (Ad-Cre). The expression of Rab6a was faintly detected at 48 h but was completely depleted at 72 h after Ad-Cre infection (Fig. 4*D*). On the other hand, Rab6b expression was undetectable in either Rab6b KO or Rab6 DKO neurons (Fig. 4*D*). Therefore, we analyzed the morphology of neurons with each genotype at 72 h after infection. Similar to the neocortex of each single KO mouse, the shape of Rab6a KO and Rab6b KO neurons resembled that of control neurons (Fig. 4*A*,*E*–*H*). Notably, in the absence of Rab6a, Rab6b was more concentrated in the Golgi area, which was similar to the localization of Rab6a in control neurons (Fig. 4*A*–*C*). In Rab6b KO neurons, Rab6a staining showed punctate signals in the soma and distal axon, similar to Rab6b signals in control neurons (Fig. 4*A*–*C*). These compensated localizations might indicate the functional redundancy of Rab6a and Rab6b to further retain the ability to generate neurons with normal shapes in each single KO.

In contrast to control and single KO neurons, Rab6 DKO neurons lost one longer neurite but contained multiple shorter neurites of similar length (Fig. 4*A*). The ratio of Stage III neurons in Rab6 DKO was <50%, and the length of the longest neurite was significantly decreased in Rab6 DKO neurons at 72 h after infection, suggesting that axonal extension was impaired (Fig. 4*E*,*F*). Conversely, the average length of minor neurites was longer in Rab6 DKO neurons than that in control and single KO neurons (Fig. 4*G*). The number of total neurites was unchanged in Rab6 DKO neurons (Fig. 4*H*). This result suggested that the function of Rab6 might be more important for the extension of generated neurites but not for the initiation of neurite formation. Taken together, our results revealed that Rab6 was crucial for neuronal development, especially for axonal extension.

Rab6 DKO neurons lose their axon–dendrite polarity

Because the impairment of axonal extension leads to the loss of neuronal polarity, we compared axon formation among neurons with each genotype by immunostaining axon-specific proteins. In most control neurons, as well as Rab6a KO and Rab6b KO neurons, only the longest neurite was positive for pMAP1B at 72 h after infection (Fig. 5*A*). However, in Rab6 DKO neurons, the soma and minor neurites were also labeled with pMAP1B antibody, indicating the loss of neuronal polarity (Fig. 5*A*). Quantitatively, the proportion of neurons with multiple pMAP1B-positive neurites was dramatically increased in Rab6 DKO neurons (Fig. 5*B*).

The formation of the growth cone at the tip of the neurite is necessary for axon outgrowth and guidance by transducing environmental signals to the cytoskeleton (Arimura and Kaibuchi, 2007; Tahirovic and Bradke, 2009). To explore the establishment of the axonal growth cone, we examined the localization of Shootin1 in primary neurons. Shootin1 specifically accumulates in the growth cone of axons at a very early stage of polarization (Toriyama et al., 2006). The accumulation of Shootin1 was observed only in the tips of axons in control, Rab6a KO, and Rab6b KO neurons, while it was observed in numerous termini of neurites in Rab6 DKO neurons (Fig. 5*C*). Similar to pMAP1B staining, the increase in the ratio of neurons with multiple Shootin1-positive neurites suggested that the polarity was disorganized in the early stage of polarization in Rab6 DKO neurons (Fig. 5*D*). Thus, these results suggest that Rab6 contributes to the establishment of axon–dendrite polarity through axonal specification and extension.

Rab6 DKO leads to the accumulation of synaptic vesicle precursors in the perinuclear region

During the establishment of neuronal polarity, the supply of membrane lipids and proteins is required for the extension of the axon and the formation of presynaptic terminals and synaptic vesicles. To specifically transport these components to the axon, accurate regulation of polarized transport to the axon is essential (Guillaud et al., 2020). Because Rab6 is known to be involved in the anterograde transport of Golgi-derived vesicles in mammalian cells, including neurons (Grigoriev et al., 2007; Nyitrai et al., 2020; Zahavi et al., 2021), we hypothesized that Rab6 promoted axonal extension through the regulation of polarized axonal transport from the Golgi apparatus. To confirm this hypothesis, we focused on the transport of three different types of vesicles that are specifically transported in the axons. First, we analyzed the distribution of plasmalemmal precursor vesicles (PPVs) in primary neurons. PPVs transport insulin-like growth factor receptors (IGF1Rs) to the growth cone and supply newly synthesized lipid membranes to facilitate plasmalemmal expansion (Pfenninger et al., 2003; Maday et al., 2014). Immunostaining of IGF1R showed similar punctate signals in both the soma and the longest neurite of neurons with all four genotypes, suggesting that the transport of PPVs was not inhibited in Rab6 DKO neurons (Fig. 6*A*). Next, we examined the distribution of dense core vesicles (DCVs). DCVs are involved in the formation of presynaptic terminals through the transport of several scaffold proteins, such as Bassoon and Piccolo, that act in the presynaptic active zone (Zhai et al., 2001; Dresbach et al., 2006). Similar to that of PPVs, the subcellular distribution of DCVs

←

ANOVA with Tukey's multiple-comparisons test). ***E***, Representative images of pMAP1B (green) staining in coronal sections of E18.5 cortices of the indicated genotypes. Deep layer neurons were stained with Tbr1 (magenta) antibody. Scale bar, 50 µm. ***F***, Quantification of the thickness of the IZ of E18.5 cerebral cortices ($n = 3$ sections from 3 brains per genotype, $^{****}p < 0.0001$, one-way ANOVA with Tukey's multiple-comparisons test). Values are represented as the mean ± SD. $^{*}p < 0.05$; $^{**}p < 0.01$; $^{***}p < 0.001$; $^{****}p < 0.0001$. Ctrl, control.

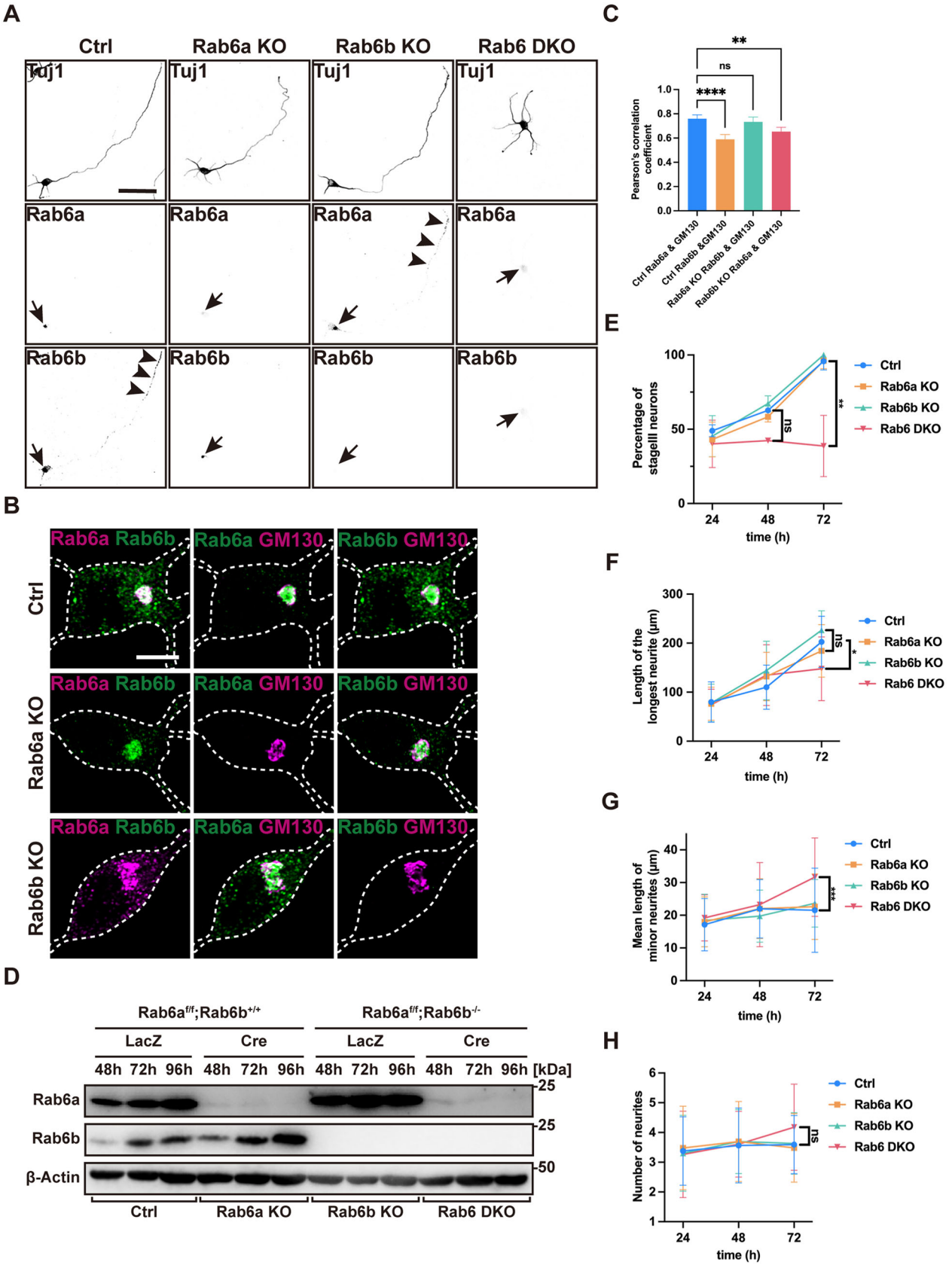

Figure 4. Rab6 DKO results in decreased axonal extension. ***A***, Representative images of Tuj1, Rab6a, and Rab6b staining in primary cortical neurons of the indicated genotypes at 72 h after adenovirus infection. Arrows indicate localization in the perinuclear region. Arrowheads indicate punctate structures in the axons. Scale bar, 50 μm. ***B***, Representative images of the subcellular distribution of Rab6a and Rab6b in the soma of primary cortical neurons of the indicated genotypes at 72 h after adenovirus infection. The Golgi apparatus was stained with GM130 antibody. Scale bar, 5 μm. ***C***, Quantification of colocalization coefficients between Rab6 and GM130 in neurons (****$p < 0.0001$, **$p = 0.0078$, one-way ANOVA with Tukey's multiple-comparisons test). ***D***, Western blot analysis of Rab6a and Rab6b expression in primary cortical neurons of the indicated genotypes. β-Actin was used as a loading control. ***E***, Quantification of the percentage of stage III neurons among cultured cortical neurons at 24, 48, and 72 h after adenovirus infection (**$p = 0.0026$, one-way ANOVA with Tukey's multiple-comparisons test). ***F***, Quantification of the

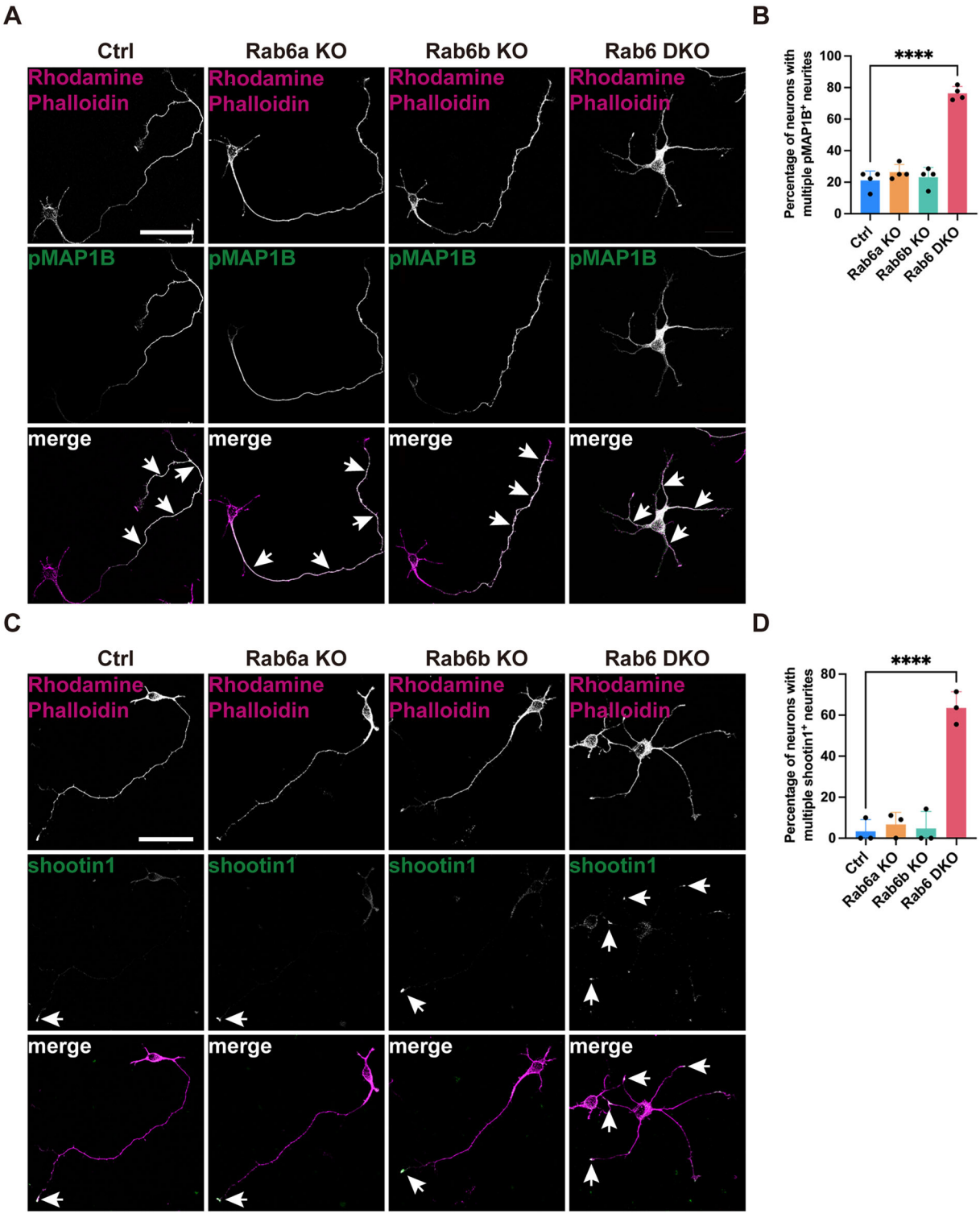

Figure 5. Rab6 DKO neurons lose their axon–dendrite polarity. ***A***, Representative images of pMAP1B (green) staining in primary cortical neurons of the indicated genotypes at 72 h after adenovirus infection. Neurites were labeled with rhodamine-phalloidin (magenta). Arrows indicate pMAP1B-positive neurites. Scale bar, 50 µm. ***B***, Quantification of the percentage of neurons with multiple pMAP1B-positive neurites at 72 h after adenovirus infection. The data were collected from four independent experiments (****$p < 0.0001$, one-way ANOVA with Tukey's multiple-comparisons test). ***C***, Representative images of Shootin1 (green) staining in primary cortical neurons of the indicated genotypes at 72 h after adenovirus infection. Neurites were labeled with rhodamine-phalloidin (magenta). Arrows indicate Shootin1 accumulation in neurite tips. Scale bar, 50 µm. ***D***, Quantification of the percentage of neurons with multiple Shootin1-positive tips of neurites at 72 h after adenovirus infection. The data were collected from three independent experiments (****$p < 0.0001$, one-way ANOVA with Tukey's multiple-comparisons test). Values are represented as the mean ± SD. ****$p < 0.0001$. Ctrl, control.

←

length of the longest neurite of cultured cortical neurons at 24, 48, and 72 h after adenovirus infection (*$p = 0.0162$, one-way ANOVA with Tukey's multiple-comparisons test). ***G***, Quantification of the average length of minor neurites of cultured cortical neurons at 24, 48, and 72 h after adenovirus infection (***$p = 0.0003$, one-way ANOVA with Tukey's multiple-comparisons test). ***H***, Quantification of the number of total neurites in cultured cortical neurons at 24, 48, and 72 h after adenovirus infection (one-way ANOVA with Tukey's multiple-comparisons test). Values are represented as the mean ± SD. *$p < 0.05$; **$p < 0.01$; ***$p < 0.001$; $p < 0.0001$; ns, not statistically significant. Ctrl, control.

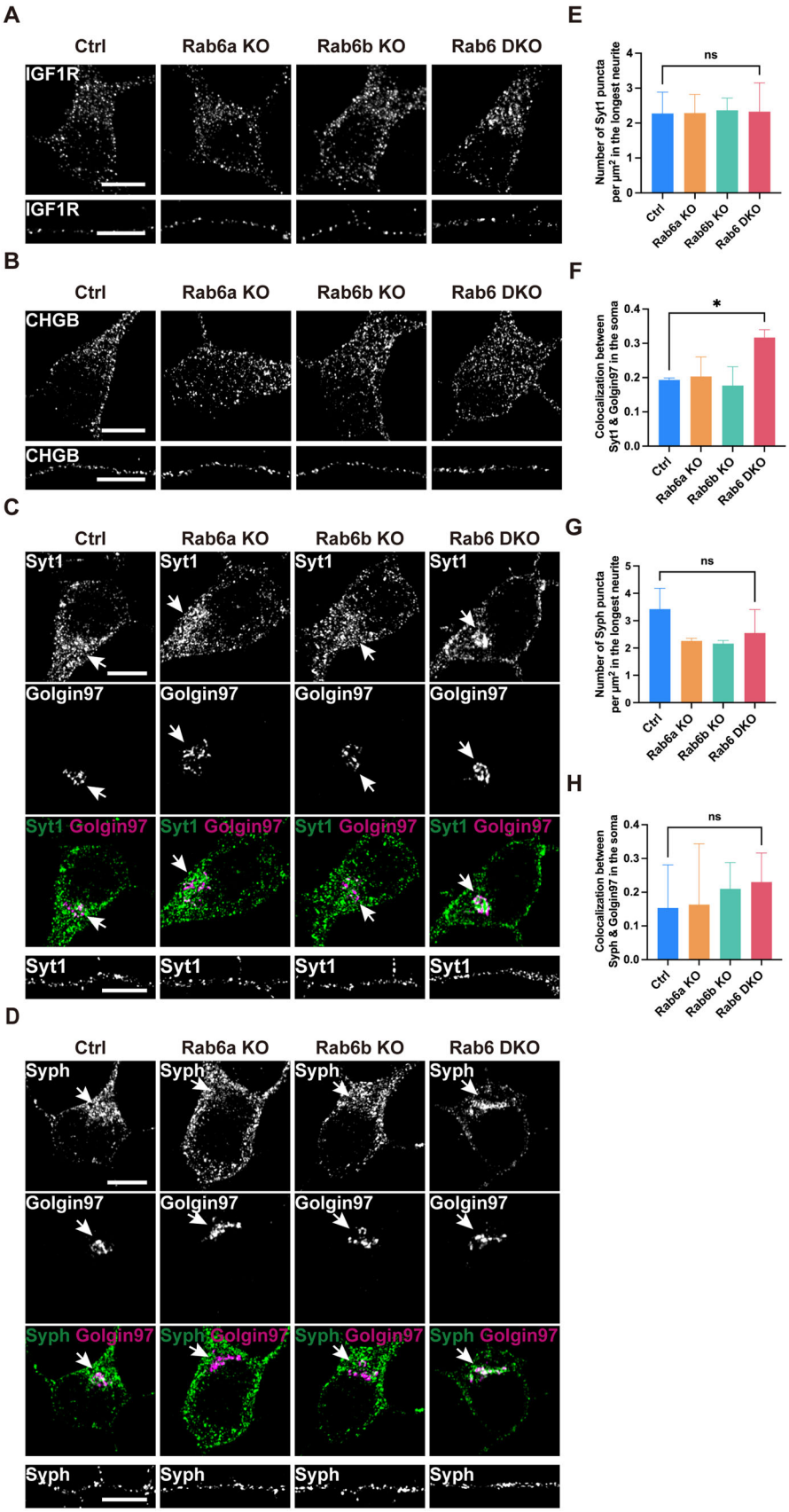

Figure 6. Rab6 DKO leads to the accumulation of synaptic vesicle precursors in the perinuclear region. ***A***, ***B***, Representative images of IGF1R (***A***) and chromogranin B (CHGB; ***B***) staining in the soma (top panels) and the longest neurite (bottom panels) of primary cortical neurons of the indicated genotypes at 72 h after adenovirus infection. Scale bars, 5 μm. ***C***, ***D***, Representative images of Synaptotagmin1 (Syt1; green in ***C***) or Synaptophysin1 (Syph; green in ***D***) staining in the soma (top panels) and the longest neurite (bottom panels) of primary cortical neurons of the indicated genotypes at 72 h after adenovirus infection. The Golgi apparatus (arrows) were stained with Golgin97 (magenta) antibody. Scale bar, 5 μm. ***E–H***, Quantifications of the

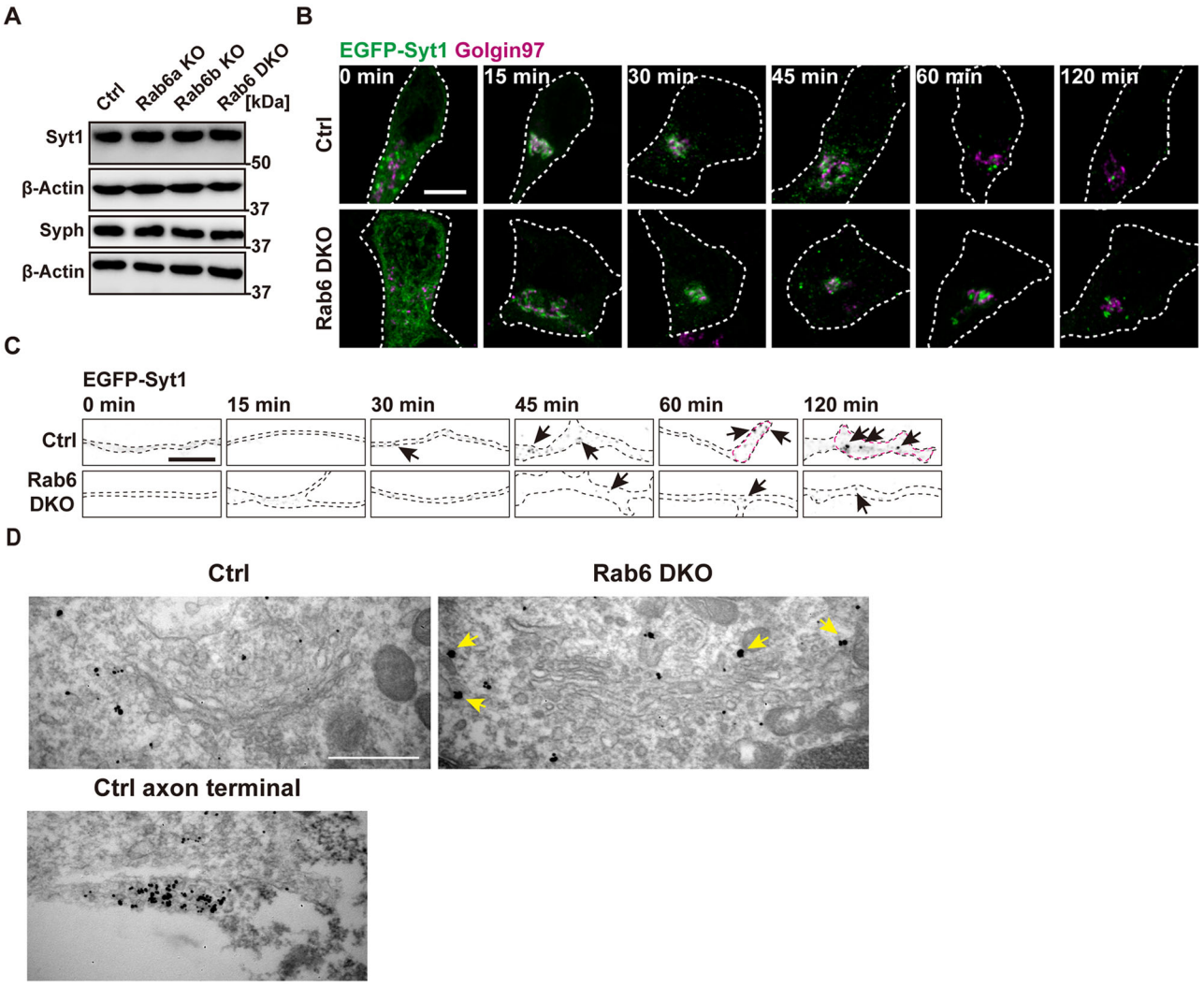

Figure 7. The accumulated synaptic vesicle precursors are located at the Golgi area in Rab6 DKO neurons. ***A***, Western blot analysis of Syt1 and Syph in DIV3 neurons of the indicated genotypes. β-Actin was used as a loading control. ***B***, ***C***, Representative images of EGFP-tagged Syt1 signals (green) and Golgin97 (magenta) staining in the soma (***B***) and the longest neurite (***C***) in control and Rab6 DKO neurons at 0, 15, 30, 45, 60, and 120 min after biotin treatment. ***B***, The soma area were surrounded by white dashed lines. ***C***, The neurites were surrounded by black dashed lines. EGFP-tagged Syt1 signals (black) are shown by arrows. Axon terminals were shown by magenta dashed lines. Scale bars, 5 µm. ***D***, Representative images of immunoelectron micrographs showing the localization of Syph in the Golgi area and axon terminal of control and Rab6 DKO neurons. Yellow arrows in Rab6 DKO panel indicate accumulated Syph adjacent to the Golgi. Scale bar, 500 nm.

labeled by chromogranin B (CHGB) was comparable among all four genotypes, suggesting that the transport of DCVs was also unaltered by Rab6 DKO (Fig. 6*B*). Finally, we compared the distribution of SVPs. SVPs transport synaptic vesicle (SV) proteins, such as synaptotagmin1 (Syt1) and synaptophysin1 (Syph), to presynaptic terminals (Santos et al., 2009; Tao-Cheng, 2020; Rizalar et al., 2021). Fusion of SVPs with the growth cone membrane is also thought to be involved in membrane expansion of the axon terminal (Igarashi et al., 1997; Nakazawa et al., 2012). To visualize SVPs, we stained primary neurons with Syt1 or Syph antibodies at 72 h after infection. In control neurons, as well as Rab6a KO and Rab6b KO neurons, Syt1 and Syph showed dispersed and punctate distributions in both the soma and axon. However, in Rab6 DKO neurons, these proteins accumulated in the perinuclear region and partially colocalized with Golgin97, which is a trans-Golgi marker (Fig. 6*C*,*D*,*F*,*H*). Moreover, the expression of these two proteins was not altered among all four genotypes, suggesting that the perinuclear accumulation of Syt1 and Syph in Rab6 DKO neurons was not due to increased expression but was likely due to transport defects (Fig. 7*A*). Although Syt1 and Syph accumulated around the Golgi area, the punctate signals of these proteins in Rab6 DKO neurites were similar to those in control axons (Fig. 6*C*–*E*,*G*). We hypothesize that these signals indicate SV proteins that are delivered before Rab6 depletion or delivered by alternate pathways. To specifically examine SVPs transport after the depletion of Rab6a and Rab6b, we utilized the retention using selective hooks (RUSH) system to probe the trafficking of EGFP-tagged Syt1 (Fig. 7*B*,*C*). In brief, EGFP-tagged Syt1 was fused with streptavidin-binding protein (SBP), and the fusion protein was retained in the endoplasmic reticulum (ER) before biotin addition. After biotin treatment, in control neurons, EGFP-tagged Syt1 concentrated in the

←

distribution of Syt1 (***E***, ***F***) or Syph (***G***, ***H***) in the longest neurite (***E***, ***G***) and the colocalization coefficients with Golgin97 (***F***, ***H***) in neurons (*$p = 0.0266$, one-way ANOVA with Tukey's multiple-comparisons test). Values are represented as the mean ± SD. *$p < 0.05$; ns, not statistically significant. Ctrl, control.

Golgi apparatus within 15 min and started the axonal transport at 30 min, as shown by the appearance of punctate signals around the Golgi (Fig. 7*C*, top panels). These EGFP-tagged Syt1 were successfully transported along the axons and accumulated in the axonal terminals in control neurons at 60 and 120 min after biotin addition (Fig. 7*C*, top panels). Meanwhile, in Rab6 DKO neurons, EGFP-tagged Syt1 also accumulated in the Golgi area within 15 min, indicating that the ER to Golgi transport was not affected (Fig. 7*B*, bottom panels). However, these proteins were retained adjacent to the Golgi at 60 and 120 min after biotin treatment, and the punctate signals were rarely seen in the neurites, representing the post-Golgi transport defect of SVPs in Rab6 DKO neurons (Fig. 7*B*,*C*, bottom panels). To explore the localization of accumulated SVP markers in Rab6 DKO neurons, we further utilized immunoelectron microscopy (Fig. 7*D*). In Rab6 DKO neurons, Syph signals were located adjacent to the Golgi stack, but not in the Golgi cisternae. Given EGFP-tagged Syt1 was colocalized with the Golgi at 15–45 min after biotin addition, it appears to be an SVP transport defect at the early stage after exit from the Golgi.

Moreover, the accumulations of SVP markers were also observed in vivo (Fig. 8). In the control neocortex, as well as

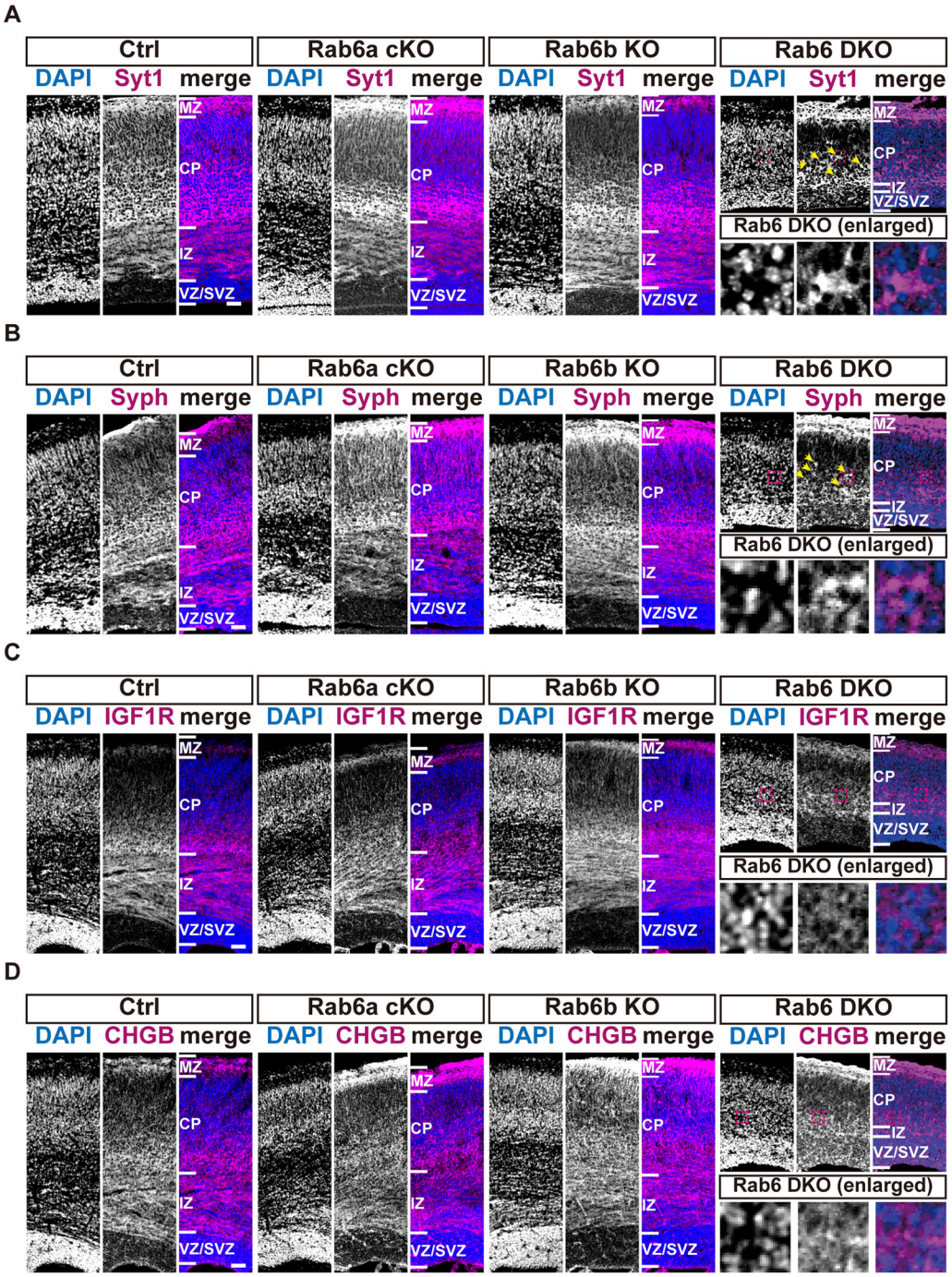

Figure 8. Rab6 DKO causes the accumulation of synaptic vesicle precursors in neuronal soma in vivo. ***A–D***, Representative images of Syt1 (magenta in ***A***), Syph (magenta in ***B***), IGF1R (magenta in ***C***), or CHGB (magenta in ***D***) in coronal sections of E18.5 cortices of the indicated genotypes. Nuclei were stained with DAPI (blue). Yellow arrows in Rab6 DKO panels indicate strongly stained neuronal soma. Bottom panels of Rab6 DKO show magnified images of the boxes surrounded by magenta dashed lines in the top panels. Scale bars, 50 µm.

Rab6a cKO and Rab6b KO, Syt1 and Syph were highly expressed in the deep layer of the CP and the IZ, reflecting the presence of SVPs within neuronal soma and axons (Fig. 8*A*,*B*). Conversely, in Rab6 DKO neocortex, prominently strongly stained soma were found in the deep layer of the CP, indicating the accumulation of SVPs in Rab6 DKO neurons (Fig. 8*A*,*B*, arrows). However, in the neocortex of all four genotypes, the DCV marker, CHGB, and PPV marker, IGF1R, were expressed similarly in the CP and the IZ (Fig. 8*C*,*D*).

To further delineate the function of Rab6 in SVP transport, we first compared the subcellular localization of Rab6 and Syt1 or Syp1 in control neurons. Rab6a and Rab6b partially colocalized with SVP markers in the Golgi area, but overlapping signals were rarely observed in the axons (Fig. 9*A*–*E*). Moreover, to

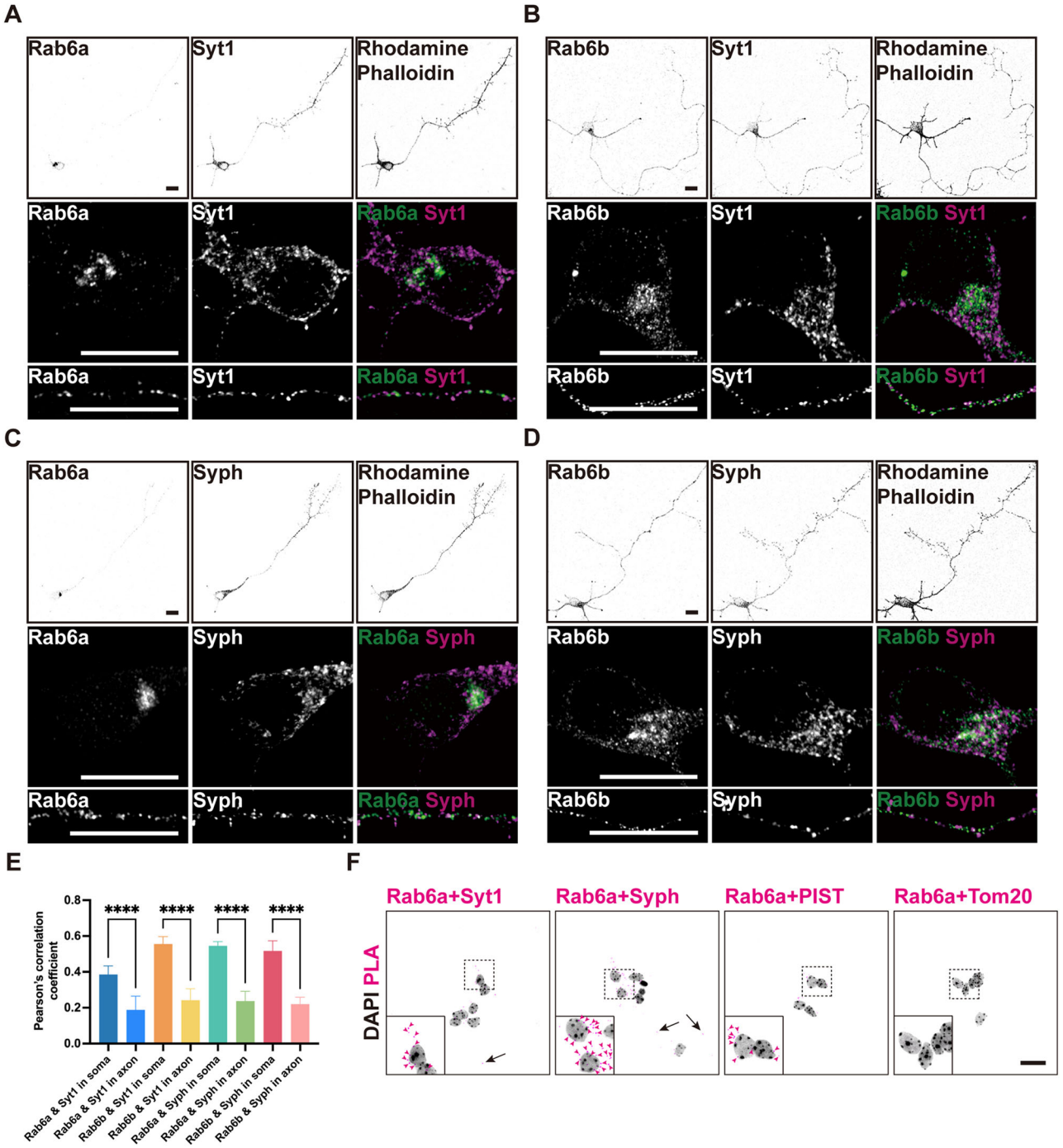

Figure 9. Rab6 does not colocalize with synaptic vesicle proteins in axon shafts. ***A–D***, Representative images of Rab6a (***A***, ***C***) or Rab6b (***B***, ***D***) and Syt1 (***A***, ***B***) or Syph (***C***, ***D***) staining in the soma (middle panels) and the axons (bottom panels) of wild-type cortical neurons (top panels) at 72 h after plating. Rhodamine-phalloidin was used to show neuronal morphology. Scale bars, 10 µm. ***E***, Quantification of colocalization coefficients between Rab6 and SVP markers in the soma and the axon in control neurons (****$p < 0.0001$, one-way ANOVA with Tukey's multiple-comparisons test). ***F***, Representative images of interaction between Rab6a and SVP markers determined by PLA. PIST, and Tom20 were used as positive and negative control, respectively. Nuclei were stained with DAPI (blue). Arrows show the PLA signals in neurites. The bottom left insets show magnified images of the boxes surrounded by dashed lines. Arrowheads in magenta show the PLA signals (magenta) in the insets. Scale bar, 2 µm. Values are represented as the mean ± SD. ****$p < 0.0001$.

explore the interaction between Rab6 and SVPs, we performed a GST pull-down assay in mouse brain homogenates by using active or inactive mutants of Rab6a and Rab6b. However, known SV protein was undetected in the mass spectrometry analysis (Table 1). Thus, we speculate Rab6 mediates SVP transport in an indirect manner by Rab6 effectors. We verified the recruitment of Rab6 near SVPs by PLA (Fig. 9*F*). The interactions between Rab6a and Syt1 or Syph predominantly occurred in the perinuclear region in neurons. These data indicate that Rab6 is more important in the initiation stage of SVP transport around the Golgi area than its trafficking in the axon shaft. Taken together, our results suggest that Rab6 promotes axonal extension by regulating the initial step of SVP transport from the TGN to the axon.

Rab6 contributes to the KIF1A recruitment during SVP transport

The recruitment of motor protein to the vesicles is critical for the initiation of polarized transport. Studies have reported that the loading of Kinesin Family Member 1A (KIF1A) contributes to the anterograde transport of SVPs (Okada et al., 1995; Yonekawa et al., 1998). We speculate that Rab6 might play a role in the loading of KIF1A to SVP carriers in neurons. To test this hypothesis, we examined the colocalization of KIF1A and Syt1 in control and Rab6 DKO neurons (Fig. 10*A*). The reduced number of overlapped signals in Rab6 DKO neurons suggests the defect of KIF1A recruitment (Fig. 10*A*,*B*). Meanwhile, the partially colocalized KIF1A and Rab33a in axons imply the axonal SVP transport might also be mediated by Rab33a (Fig. 10*C*), which is consistent with a previous report (Nakazawa et al., 2012). Though Rab6 signals were widely detected in the neurites, many of them are negative for SVP markers (Fig. 9*A*–*E*). This raises the question what cargoes are transported by Rab6-positive vesicles. A neurotrophin receptor, TrkB, was reported to be transported by Rab6 (Zahavi et al., 2021). However, when we performed the localization study of Rab6 and TrkB by immunostaining, only a small portion of TrkB was positive for Rab6a or Rab6b (Fig. 10*D*). Moreover, TrkB showed similar distribution between control neurons and Rab6 DKO neurons (Fig. 10*E*–*G*). Thus, Rab6 has minimal impact on TrkB localization. Taken together, Rab6 might function in the recruitment of motor proteins in SVP transport in neurons.

Table 1. Rab6 interactors identified by pull-down screening in mouse brain homogenates

#	Identified proteins (40/51)	Accession number	Molecular weight
1	RAB6, member RAS oncogene family, isoform CRA_c OS = Mus musculus OX = 10,090 GN = Rab6a PE = 2 SV = 1	Q3U4W5_MOUSE	24 kDa
2	Tubulin β-4B chain OS = Mus musculus OX = 10,090 GN = Tubb4b PE = 1 SV = 1	TBB4B_MOUSE	50 kDa
3	Dynactin subunit 2 OS = Mus musculus OX = 10,090 GN = Dctn2 PE = 1 SV = 3	DCTN2_MOUSE (+1)	44 kDa
4	Carbonyl reductase 1 OS = Mus musculus OX = 10,090 GN = Cbr1 PE = 1 SV = 1	B2RXY7_MOUSE (+1)	31 kDa
5	Glutathione S-transferase Mu 1 OS = Mus musculus OX = 10,090 GN = Gstm1 PE = 1 SV = 2	GSTM1_MOUSE	26 kDa
6	Tubulin α-1B chain OS = Mus musculus OX = 10,090 GN = Tuba1b PE = 1 SV = 2	TBA1B_MOUSE	50 kDa
7	RAB6B, member RAS oncogene family OS = Mus musculus OX = 10,090 GN = Rab6b PE = 1 SV = 1	Q0PD53_MOUSE (+1)	23 kDa
8	Rab GDP dissociation inhibitor beta OS = Mus musculus OX = 10,090 GN = Gdi2 PE = 1 SV = 1	GDIB_MOUSE (+3)	51 kDa
9	Phosphomannomutase 1 OS = Mus musculus OX = 10,090 GN = Pmm1 PE = 1 SV = 1	PMM1_MOUSE (+1)	30 kDa
10	Beta-centractin OS = Mus musculus OX = 10,090 GN = Actr1b PE = 1 SV = 1	ACTY_MOUSE	42 kDa
11	Glutathione S-transferase P 1 OS = Mus musculus OX = 10,090 GN = Gstp1 PE = 1 SV = 2	GSTP1_MOUSE	24 kDa
12	Dynactin subunit 1 OS = Mus musculus OX = 10,090 GN = Dctn1 PE = 1 SV = 3	DCTN1_MOUSE (+3)	142 kDa
13	Myelin basic protein (Fragment) OS = Mus musculus OX = 10,090 GN = Mbp PE = 1 SV = 1	F6RT34_MOUSE (+1)	23 kDa
14	ELKS/Rab6-interacting/CAST family member 1 OS = Mus musculus OX = 10,090 GN = Erc1 PE = 1 SV = 1	F8VPM7_MOUSE (+3)	128 kDa
15	Elongation factor 1-α 2 OS = Mus musculus OX = 10,090 GN = Eef1a2 PE = 1 SV = 1	EF1A2_MOUSE	50 kDa
16	Actin, cytoplasmic 1 OS = Mus musculus OX = 10,090 GN = Actb PE = 1 SV = 1	ACTB_MOUSE (+12)	42 kDa
17	Tubulin β-2A chain OS = Mus musculus OX = 10,090 GN = Tubb2a PE = 1 SV = 1	TBB2A_MOUSE	50 kDa
18	Glutathione S-transferase A4 OS = Mus musculus OX = 10,090 GN = Gsta4 PE = 1 SV = 3	GSTA4_MOUSE	26 kDa
19	Tubulin alpha chain (Fragment) OS = Mus musculus OX = 10,090 GN = Tuba4a PE = 1 SV = 1	A0A0A0MQA5_MOUSE (+1)	53 kDa
20	Elongation factor 1-γ OS = Mus musculus OX = 10,090 GN = Eef1g PE = 1 SV = 3	EF1G_MOUSE (+1)	50 kDa
21	Tubulin α-1A chain OS = Mus musculus OX = 10,090 GN = Tuba1a PE = 1 SV = 1	TBA1A_MOUSE	50 kDa
22	Protein bicaudal D homolog 1 OS = Mus musculus OX = 10,090 GN = Bicd1 PE = 1 SV = 1	B2KG46_MOUSE (+3)	111 kDa
23	Microtubule-associated protein 2 OS = Mus musculus OX = 10,090 GN = Map2 PE = 1 SV = 2	MTAP2_MOUSE	199 kDa
24	Alpha-centractin OS = Mus musculus OX = 10,090 GN = Actr1a PE = 1 SV = 1	ACTZ_MOUSE	43 kDa
25	Rab GDP dissociation inhibitor alpha OS = Mus musculus OX = 10,090 GN = Gdi1 PE = 1 SV = 3	GDIA_MOUSE	51 kDa
26	Eukaryotic translation elongation factor 1 beta 2 OS = Mus musculus OX = 10,090 GN = Eef1b2 PE = 1 SV = 1	A0A087WS46_MOUSE (+1)	20 kDa
27	Glutathione S-transferase LANCL1 OS = Mus musculus OX = 10,090 GN = Lancl1 PE = 1 SV = 1	LANC1_MOUSE	45 kDa
28	Tubulin β-3 chain OS = Mus musculus OX = 10,090 GN = Tubb3 PE = 1 SV = 1	TBB3_MOUSE	50 kDa
29	Ras-related protein Rab-6A OS = Mus musculus OX = 10,090 GN = Rab6a PE = 1 SV = 1	D3YV69_MOUSE	20 kDa
30	Protein bicaudal D homolog 2 OS = Mus musculus OX = 10,090 GN = Bicd2 PE = 1 SV = 1	BICD2_MOUSE	93 kDa
31	Polymerase δ-interacting protein 3 OS = Mus musculus OX = 10,090 GN = Poldip3 PE = 1 SV = 1	PDIP3_MOUSE (+3)	46 kDa
32	Glutathione S-transferase (Fragment) OS = Mus musculus OX = 10,090 GN = Gstm5 PE = 1 SV = 1	E9PVM7_MOUSE (+1)	26 kDa
33	Dynactin subunit 4 OS = Mus musculus OX = 10,090 GN = Dctn4 PE = 1 SV = 1	DCTN4_MOUSE (+1)	53 kDa
34	Golgi-associated PDZ and coiled-coil motif-containing protein OS = Mus musculus OX = 10,090 GN = Gopc PE = 1 SV = 1	GOPC_MOUSE (+1)	51 kDa
35	Tubulin β-4A chain OS = Mus musculus OX = 10,090 GN = Tubb4a PE = 1 SV = 3	TBB4A_MOUSE	50 kDa
36	Heat shock cognate 71 kDa protein OS = Mus musculus OX = 10,090 GN = Hspa8 PE = 1 SV = 1	HSP7C_MOUSE (+10)	71 kDa
37	F-actin-capping protein subunit α-2 OS = Mus musculus OX = 10,090 GN = Capza2 PE = 1 SV = 3	CAZA2_MOUSE (+1)	33 kDa
38	14-3-3 protein epsilon OS = Mus musculus OX = 10,090 GN = Ywhae PE = 1 SV = 1	1433E_MOUSE (+4)	29 kDa
39	BTB/POZ domain-containing adapter for CUL3-mediated RhoA degradation protein 3 OS = Mus musculus OX = 10,090 GN = Kctd10 PE = 1 SV = 1	BACD3_MOUSE (+1)	36 kDa
40	Solute carrier family 25 member 48 OS = Mus musculus OX = 10,090 GN = Slc25a48 PE = 1 SV = 2	S2548_MOUSE	33 kDa

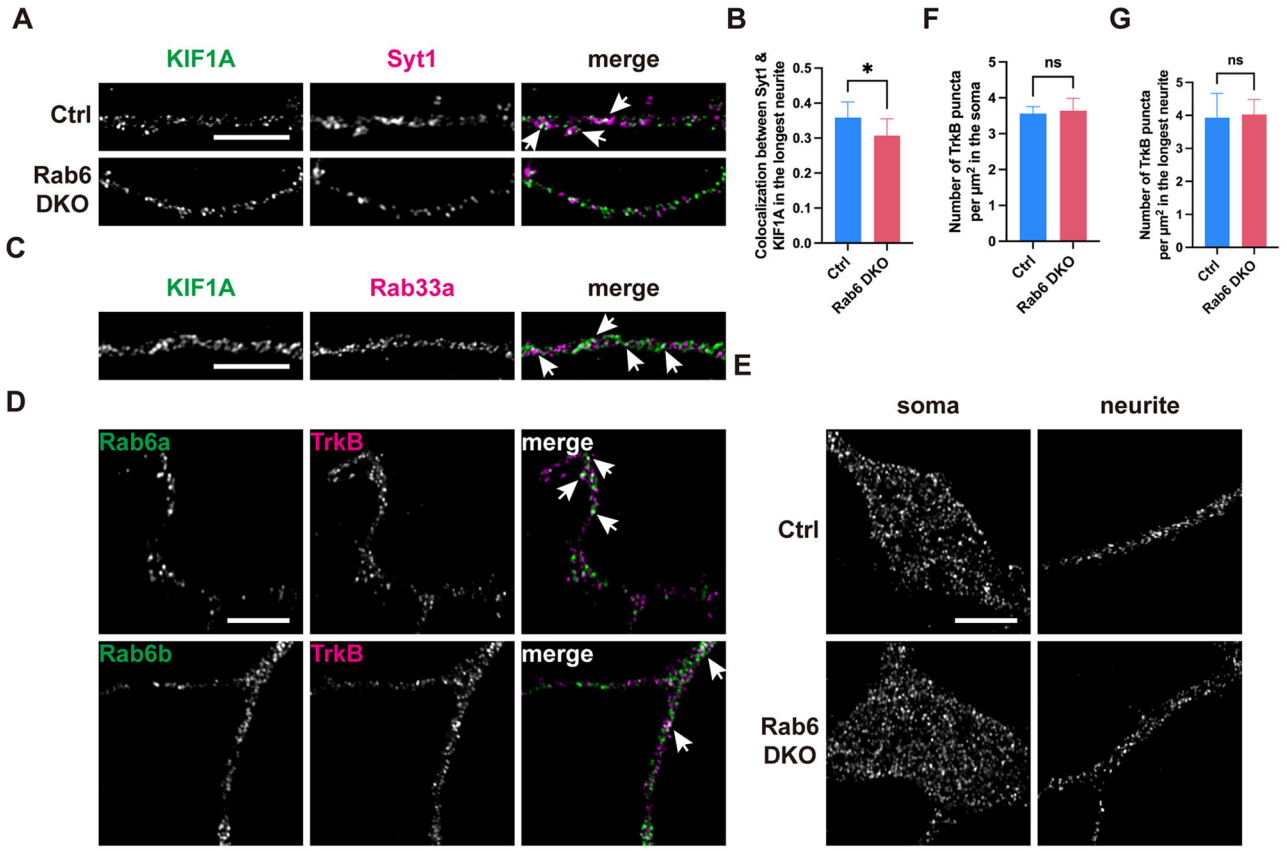

Figure 10. Rab6 partially colocalizes with TrkB in the axons. ***A***, Representative images of KIF1A (green) and Syt1 (magenta) staining in the longest neurite of control and Rab6 DKO neurons. Arrows show overlapped signals. Scale bar, 5 μm. ***B***, Quantification of colocalization coefficients between Syt1 and KIF1A in the longest neurite of control and Rab6 DKO neurons (*$p = 0.0488$, unpaired *t* test). ***C***, Representative images of KIF1A (green) and Rab33a (magenta) staining in the control axons. Arrows show overlapped signals. Scale bar, 5 μm. ***D***, Representative images of Rab6a or Rab6b (green) and TrkB (magenta) staining in the control axons. Arrows show overlapped signals. Scale bar, 5 μm. ***E***, Representative images of TrkB staining in the soma and the longest neurite of control and Rab6 DKO neurons. Scale bar, 5 μm. ***F***, ***G***, Quantification of distributions of TrkB in the soma (***F***) or the longest neurite (***G***) of control and Rab6 DKO neurons (unpaired *t* test). Values are represented as the mean ± SD. *$p < 0.05$; ns, not statistically significant. Ctrl, control.

Rab6 DKO causes lysosomal enlargement and accumulation in the soma

In addition to anterograde vesicular transport from the TGN to the plasma membrane, Rab6 was also reported to be involved in retrograde transport from the endosome to the Golgi apparatus (Mallard et al., 2002; Monier et al., 2002). We next examined whether the endocytic and lysosomal degradation pathways were affected in Rab6 DKO neurons. First, we characterized the distribution of early endosomes (EEs) in primary neurons by staining the EE marker, early endosome antigen 1 (EEA1). EEA1-positive EEs showed comparable, spherical signals throughout the somatodendritic compartments of primary neurons with all four genotypes (Fig. 11*A*). Next, we stained neurons with CD71/transferrin receptor 1 antibody to visualize the distribution of recycling endosomes (REs). These CD71-positive REs were enriched in the soma and found in the dendrites of control neurons. The localization of REs was not changed in Rab6 DKO neurons compared with control and single KO neurons (Fig. 11*B*). These results suggested that endocytic and recycling pathways were not influenced by the depletion of Rab6a/b in primary neurons. Finally, we analyzed the identity and localization of lysosomes by immunostaining for lysosomal-associated membrane protein 1 (LAMP1). In control neurons, as well as Rab6a KO and Rab6b KO neurons, LAMP1 staining showed dispersed vesicular signals and was enriched in the perinuclear region. However, in Rab6 DKO neurons, lysosomes were significantly enlarged and more accumulated than those in control neurons (Fig. 11*C–H*). Given the relatively unaltered amount and distribution of the other endocytic compartments, we speculate that the enlargement and accumulation of lysosomes were likely due to lysosomal dysfunction and/or increased mistargeting of accumulated SVPs to lysosomes. To examine the lysosomal function, we compared the lysosomal acidity in control and Rab6 DKO neurons using the Lysosomal Acidic pH Detection Kit. In control neurons, pHLys Red dye accumulated in acidic lysosomes and disappeared after the treatment of a lysosomal inhibitor, bafilomycin A1 (BafA1; Fig. 12*A*). However, pHLys Red fluorescence diminished after Rab6 depletion. In particular, some enlarged lysosomes were unstained, indicating the impaired acidification and dysfunction of lysosomes in Rab6 DKO neurons. Meanwhile, the expression and maturation of lysosomal hydrolase, Cathepsin D, was similar among all four genotypes in DIV3 neurons (Fig. 12*B*). The apparently normal maturation of Cathepsin D in Rab6 DKO neurons might be explained by the following reasons. In our experiment system, Rab6a is completely depleted at 72 h after lentivirus treatment. As lysosomal acidification is likely to be sensitive to the depletion of Rab6, it is shown to be impaired at this point (Fig. 12*A*). However, as the maturation of lysosomal hydrolases is likely to require an acidified environment for longer period, the defect of hydrolase maturation often lags behind the acidification defect (Fig. 12*B*). When we further investigated whether accumulated

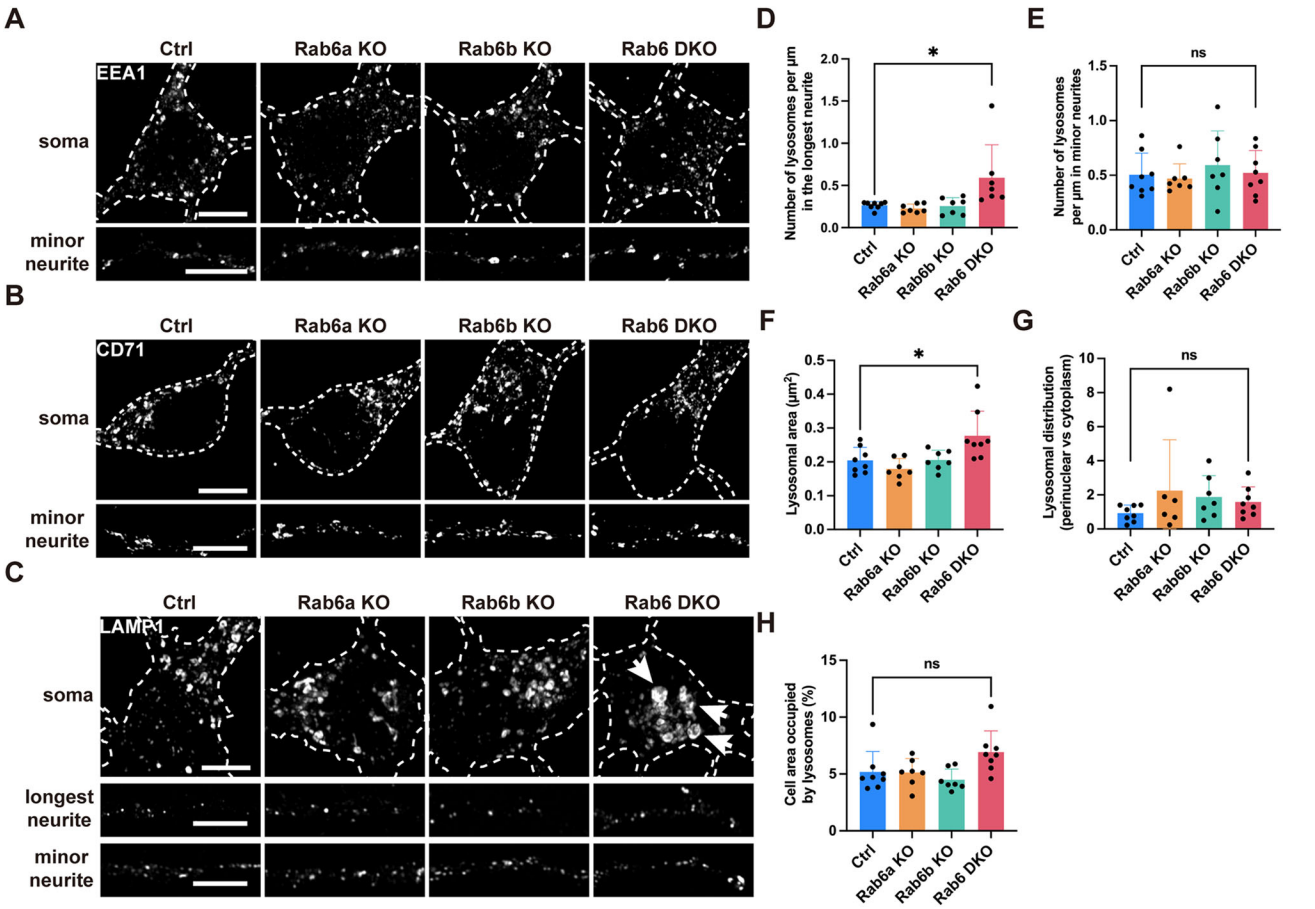

Figure 11. Rab6 DKO causes lysosomal enlargement and accumulation in the soma. ***A***, ***B***, Representative images of EEA1 (***A***) or CD71 (***B***) staining in the soma (top panels) and dendrites (bottom panels) of cortical neurons of the indicated genotypes at 72 h after adenovirus infection. Scale bars, 5 μm. ***C***, Representative images of LAMP1 staining in the soma, the longest neurite, and a minor neurite of primary cortical neurons of the indicated genotypes at 72 h after adenovirus infection. Arrows show enlarged lysosomes in the soma of Rab6 DKO neurons. Scale bars, 5 μm. ***D–H***, Quantifications of the distribution and the size of lysosomes in cortical neurons of indicated genotypes at 72 h after adenovirus infection (*$p = 0.0213$ in ***D***, *$p = 0.0232$ in ***F***, one-way ANOVA with Tukey's multiple-comparisons test for all). Values are represented as the mean ± SD. *$p < 0.05$; ns, not statistically significant. Ctrl, control.

SVPs mistarget to lysosomes, we found that accumulated Syt1 rarely overlapped with lysosomes in the presence or absence of BafA1 in Rab6 DKO neurons (Fig. 12*C*). Moreover, using the RUSH system, we found the accumulated EGFP-tagged Syt1 was not mistargeted to lysosomes at 60 and 120 min after biotin addition in Rab6 DKO neurons (Fig. 12*D*). Taken together, Rab6 DKO causes lysosomal dysfunction and expansion in neurons, which seems independent of SVP accumulation.

Discussion

In this study, our findings provide the first evidence that Rab6 plays a crucial role in neuronal polarization and subsequent neocortical IZ formation in vivo. Rab6 promotes axon specification and extension through the regulation of post-Golgi polarized transport of SVPs in developing neurons (Fig. 13). By analyzing similar Rab6 DKO mice, we and the other group revealed that Rab6 regulates polarized transport in different types of cells in the developing brain, such as NPCs and neurons (Brault et al., 2022). These reports indicate the functional significance of Rab6 in the development of the mammalian brain.

We proved that the deletion of Rab6a and Rab6b causes abnormal accumulation of SVPs in the Golgi area in vitro and in vivo, while the distribution of PPVs or DCVs was indistinguishable from that of control neurons and neocortex (Figs. 6–8). These results suggest that Rab6 is particularly important for the post-Golgi transport of SVPs. The axonal transport of SVPs and their fusion at the growth cone were necessary for axonal extension (Igarashi et al., 1997; Nakazawa et al., 2012). Therefore, we conclude that the accumulation of SVPs in the soma is the major cause of the loss of polarity in Rab6 DKO neurons.

In control neurons, the localization of Rab6a and Rab6b was enriched around the Golgi, and their signals in axons were not colocalized with those of SVPs (Figs. 4*B*, 9). In addition, SVPs accumulated adjacent to the Golgi in Rab6 DKO neurons (Figs. 6, 7). These results suggested that Rab6 might regulate the initial steps of the transport pathway, such as the recruitment of motor proteins. In axonal transport pathways, the molecular functions of motor proteins, such as kinesin and dynein, are well characterized (Hirokawa et al., 2010; Maday et al., 2014). Among motor proteins, the kinesin-3 family members KIF1A and KIF1Bβ are required for the anterograde axonal transport of SVPs (Okada et al., 1995; Yonekawa et al., 1998; Zhao et al., 2001). In our study, the colocalization between SVPs and KIF1A diminished after Rab6 DKO in axon shafts (Figs. 10*A*, *B*). We therefore hypothesized that Rab6 could contribute to the coupling between SVPs and kinesin-3. A previous report indicated that Rab6 directly interacts with KIF20A (kinesin-6) to regulate vesicle fission from the Golgi in HeLa cells

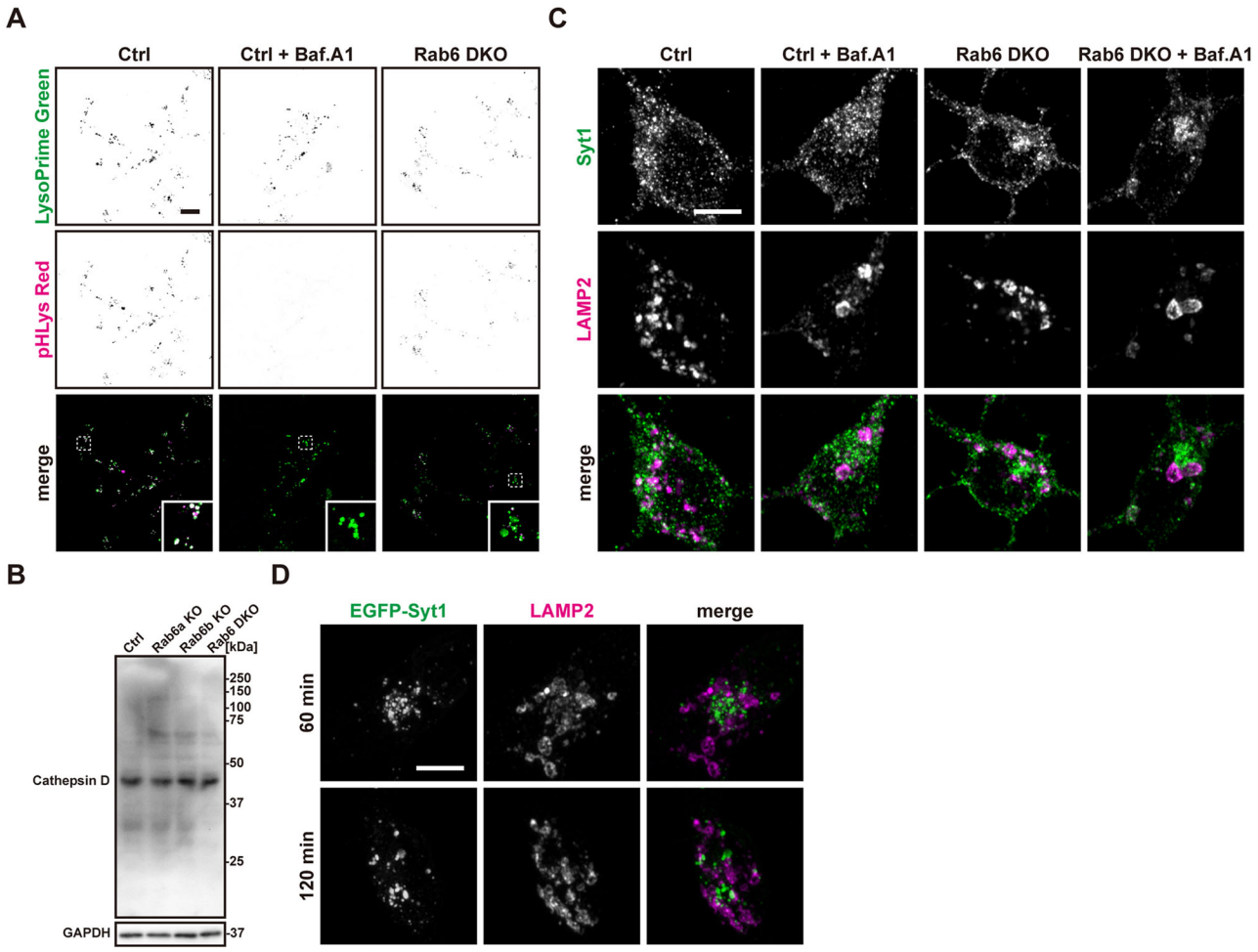

Figure 12. Rab6 DKO causes the defect of lysosomal acidification in neurons. ***A***, Representative images of lysosomal acidification visualized by Lysosomal Acidic pH Detection Kit in control and Rab6 DKO neurons. Bafilomycin A1 (Baf.A1) was used as a lysosomal inhibitor. The bottom right insets in the bottom panels show magnified images of the boxes surrounded by dashed lines. Scale bar, 5 µm. ***B***, Western blot analysis of Cathepsin D in cortical neurons of the indicated genotypes at 72 h after adenovirus infection. GAPDH was used as a loading control. ***C***, Representative images of Syt1 (green) and LAMP2 (magenta) staining in the soma of control and Rab6 DKO neurons in the presence or absence of bafilomycin A1. Scale bar, 5 µm. ***D***, Representative images of EGFP-tagged Syt1 signals (green) and LAMP2 (magenta) staining in the soma of Rab6 DKO neurons at 60 and 120 min after biotin treatment. Scale bar, 5 µm.

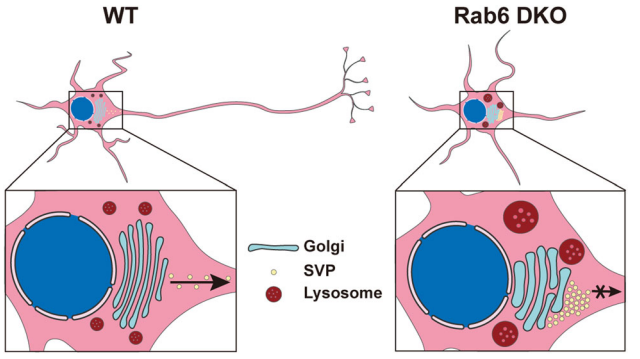

Figure 13. A schematic model showing the function of Rab6 in SVP anterograde transport in neurons. WT, wild type; SVP, synaptic vesicle precursor.

(Miserey-Lenkei et al., 2017). In addition to direct interactions, Bicaudal-D (BICD) family members, which are known as effector proteins of Rab6, are candidates for this coupling process because BICD proteins can bind to kinesin motors, including kinesin-3 (Grigoriev et al., 2007; Schlager et al., 2010). However, the functions of BICD proteins in the anterograde transport pathway remain unclear. In addition to BICD proteins, a number of effector proteins of Rab6 have been identified to date (Goud et al., 2018). Thus, Rab6 may interact with kinesin-3 directly or indirectly to couple SVPs with motor proteins in neurons. Accordingly, further investigations are needed to determine the interaction between kinesin-3 or kinesin-6 and the Rab6 or Rab6 effector for the anterograde axonal transport of SVPs. Moreover, it was reported that Rab33a is involved in the axonal transport and fusion steps of SVPs in developing neurons (Nakazawa et al., 2012). In our study, Rab33a was partially colocalized with KIF1A in axons (Fig. 10C). Therefore, Rab6 may function upstream of Rab33a in SVP transport.

Although Rab6 DKO resulted in the significant accumulation of SVPs adjacent to the Golgi, a few SVPs were still detected in Rab6 DKO neurites (Figs. 6, 7). These SVPs might be transported via other Rab proteins. A recent study reported that Rab2 plays an important role in the biogenesis and axonal transport of SVPs in *Drosophila* larval neurons (Götz et al., 2021). However, the function of Rab2 in mammalian neurons is still unclear. Therefore, further studies will be necessary to determine the function of Rab2 and the functional connection between Rab2 and Rab6 for SVP transport in mammalian neurons.

A recent study showed that Rab6-positive vesicles transported newly synthesized TrkB, which is a neurotrophin receptor, from the Golgi to the axon terminal (Zahavi et al., 2021). Our immunofluorescence results also showed that Rab6-positive vesicles were rarely positive for SVP markers, but some of them were positive for TrkB in control axons (Figs. 9, 10*D*). However, immunostaining of TrkB showed similar punctate signals in both control and Rab6 DKO neurons (Fig. 10*E–G*). We speculate that Rab6 functions only in the anterograde transport of newly synthesized TrkB and that a relatively small amount of TrkB was anterogradely transported. This observation seems to be consistent with the previous results (Zahavi et al., 2021). Altogether, we hypothesize that Rab6-positive vesicles lacking SVP proteins in control axons may indicate the transport vesicles containing neurotrophin receptors.

We found enlarged lysosomes in Rab6 DKO neurons, whereas the structures and distribution of EEs and REs were not altered in Rab6 DKO neurons (Fig. 11). This result suggested that the expansion of lysosomes might not be due to defects in endocytic pathways. In our previous study, we found that impaired apical transport led to enlarged lysosomes in intestinal epithelial cells (IECs) in Rab8 KO mice (Sato et al., 2007). In Rab8 KO IECs, some apical proteins, such as several peptidases and transporters, were likely to be missorted to lysosomes, which resulted in the abnormal expansion of lysosomes (Sato et al., 2007). However, in Rab6 DKO neurons, SVPs were not mistargeted to lysosomes, while the lysosomal acidification was impaired (Fig. 12). Therefore, impaired acidification and dysfunction may result in the accumulation of undegraded lysosomal content and further abnormal expansion.

In summary, our results indicate that Rab6 serves as a key regulator of the polarized axonal transport pathway, particularly at the early-stage post-Golgi transport of SVPs, which is vital for the establishment of neuronal axon–dendrite polarity during neocortex development. However, the detailed molecular mechanism of SVP transport and lysosomal homeostasis mediated by Rab6 remains unknown. Addressing and solving this issue will be valuable for understanding brain development in the future.

References

Arimura N, et al. (2009) Anterograde transport of TrkB in axons is mediated by direct interaction with Slp1 and Rab27. Dev Cell 16:675–686.

Arimura N, Kaibuchi K (2007) Neuronal polarity: from extracellular signals to intracellular mechanisms. Nat Rev Neurosci 8:194–205.

Avriyanti E, Atik N, Kunii M, Furumoto N, Iwano T, Yoshimura S, Harada R, Harada A (2015) Functional redundancy of protein kinase D1 and protein kinase D2 in neuronal polarity. Neurosci Res 95:12–20.

Barnes AP, Polleux F (2009) Establishment of axon-dendrite polarity in developing neurons. Annu Rev Neurosci 32:347–381.

Bentley M, Banker G (2016) The cellular mechanisms that maintain neuronal polarity. Nat Rev Neurosci 17:611–622.

Boyne LJ, Martin K, Hockfield S, Fischer I (1995) Expression and distribution of phosphorylated MAP1B in growing axons of cultured hippocampal neurons. J Neurosci Res 40:439–450.

Bradke F, Dotti CG (1997) Neuronal polarity: vectorial cytoplasmic flow precedes axon formation. Neuron 19:1175–1186.

Brault JB, et al. (2022) RAB6 and dynein drive post-Golgi apical transport to prevent neuronal progenitor delamination. EMBO Rep 23:e54605.

Butts T, Green MJ, Wingate RJ (2014) Development of the cerebellum: simple steps to make a 'little brain'. Development 141:4031–4041.

Dresbach T, Torres V, Wittenmayer N, Altrock WD, Zamorano P, Zuschratter W, Nawrotzki R, Ziv NE, Garner CC, Gundelfinger ED (2006) Assembly of active zone precursor vesicles: obligatory trafficking of presynaptic cytomatrix proteins Bassoon and Piccolo via a trans-Golgi compartment. J Biol Chem 281:6038–6047.

Echard A, Opdam FJ, de Leeuw HJ, Jollivet F, Savelkoul P, Hendriks W, Voorberg J, Goud B, Fransen JA (2000) Alternative splicing of the human Rab6A gene generates two close but functionally different isoforms. Mol Biol Cell 11:3819–3833.

Götz TWB, Puchkov D, Lysiuk V, Lützkendorf J, Nikonenko AG, Quentin C, Lehmann M, Sigrist SJ, Petzoldt AG (2021) Rab2 regulates presynaptic precursor vesicle biogenesis at the trans-Golgi. J Cell Biol 220: e202006040.

Goud B, Liu S, Storrie B (2018) Rab proteins as major determinants of the Golgi complex structure. Small GTPases 9:66–75.

Greig LC, Woodworth MB, Galazo MJ, Padmanabhan H, Macklis JD (2013) Molecular logic of neocortical projection neuron specification, development and diversity. Nat Rev Neurosci 14:755–769.

Grigoriev I, et al. (2007) Rab6 regulates transport and targeting of exocytotic carriers. Dev Cell 13:305–314.

Guillaud L, El-Agamy SE, Otsuki M, Terenzio M (2020) Anterograde axonal transport in neuronal homeostasis and disease. Front Mol Neurosci 13: 556175.

Hirokawa N, Niwa S, Tanaka Y (2010) Molecular motors in neurons: transport mechanisms and roles in brain function, development, and disease. Neuron 68:610–638.

Homma Y, Kinoshita R, Kuchitsu Y, Wawro PS, Marubashi S, Oguchi ME, Ishida M, Fujita N, Fukuda M (2019) Comprehensive knockout analysis of the Rab family GTPases in epithelial cells. J Cell Biol 218: 2035–2050.

Igarashi M, Tagaya M, Komiya Y (1997) The soluble N-ethylmaleimide-sensitive factor attached protein receptor complex in growth cones: molecular aspects of the axon terminal development. J Neurosci 17: 1460–1470.

Iwaki A, Moriwaki K, Sobajima T, Taniguchi M, Yoshimura SI, Kunii M, Kanda S, Kamada Y, Miyoshi E, Harada A (2020) Loss of Rab6a in the small intestine causes lipid accumulation and epithelial cell death from lactation. FASEB J 34:9450–9465.

Kon E, Cossard A, Jossin Y (2017) Neuronal polarity in the embryonic mammalian cerebral cortex. Front Cell Neurosci 11:163.

Kunii M, et al. (2021) SNAP23 deficiency causes severe brain dysplasia through the loss of radial glial cell polarity. J Cell Biol 220:e201910080.

Maday S, Twelvetrees AE, Moughamian AJ, Holzbaur EL (2014) Axonal transport: cargo-specific mechanisms of motility and regulation. Neuron 84:292–309.

Mallard F, Tang BL, Galli T, Tenza D, Saint-Pol A, Yue X, Antony C, Hong W, Goud B, Johannes L (2002) Early/recycling endosomes-to-TGN transport involves two SNARE complexes and a Rab6 isoform. J Cell Biol 156:653–664.

Meijering E, Jacob M, Sarria JC, Steiner P, Hirling H, Unser M (2004) Design and validation of a tool for neurite tracing and analysis in fluorescence microscopy images. Cytometry A 58:167–176.

Miserey-Lenkei S, et al. (2017) Coupling fission and exit of RAB6 vesicles at Golgi hotspots through kinesin-myosin interactions. Nat Commun 8: 1254.

Monier S, Jollivet F, Janoueix-Lerosey I, Johannes L, Goud B (2002) Characterization of novel Rab6-interacting proteins involved in endosome-to-TGN transport. Traffic 3:289–297.

Nakajo A, Yoshimura S, Togawa H, Kunii M, Iwano T, Izumi A, Noguchi Y, Watanabe A, Goto A, Sato T (2016) EHBP1L1 coordinates Rab8 and Bin1 to regulate apical-directed transport in polarized epithelial cells. J Cell Biol 212:297–603.

Nakazawa H, Sada T, Toriyama M, Tago K, Sugiura T, Fukuda M, Inagaki N (2012) Rab33a mediates anterograde vesicular transport for membrane exocytosis and axon outgrowth. J Neurosci 32:12712–12725.

Nyitrai H, Wang SSH, Kaeser PS (2020) ELKS1 captures Rab6-marked vesicular cargo in presynaptic nerve terminals. Cell Rep 31:107712.

Okada Y, Yamazaki H, Sekine-Aizawa Y, Hirokawa N (1995) The neuron-specific kinesin superfamily protein KIF1A is a unique monomeric motor for anterograde axonal transport of synaptic vesicle precursors. Cell 81: 769–780.

Opdam FJ, Echard A, Croes HJ, van den Hurk JA, van de Vorstenbosch RA, Ginsel LA, Goud B, Fransen JA (2000) The small GTPase Rab6B, a novel Rab6 subfamily member, is cell-type specifically expressed and localised to the Golgi apparatus. J Cell Sci 113:2725–2735.

Pfenninger KH, Laurino L, Peretti D, Wang X, Rosso S, Morfini G, Cáceres A, Quiroga S (2003) Regulation of membrane expansion at the nerve growth cone. J Cell Sci 116:1209–1217.

Radler MR, Suber A, Spiliotis ET (2020) Spatial control of membrane traffic in neuronal dendrites. Mol Cell Neurosci 105:103492.
Rizalar FS, Roosen DA, Haucke V (2021) A presynaptic perspective on transport and assembly mechanisms for synapse formation. Neuron 109:27–41.
Santos MS, Li H, Voglmaier SM (2009) Synaptic vesicle protein trafficking at the glutamate synapse. Neuroscience 158:189–203.
Sato-Yoshitake R, Shiomura Y, Miyasaka H, Hirokawa N (1989) Microtubule-associated protein 1B: molecular structure, localization, and phosphorylation-dependent expression in developing neurons. Neuron 3:229–238.
Sato T, et al. (2007) The Rab8 GTPase regulates apical protein localization in intestinal cells. Nature 448:366–369.
Schlager MA, et al. (2010) Pericentrosomal targeting of Rab6 secretory vesicles by Bicaudal-D-related protein 1 (BICDR-1) regulates neuritogenesis. Embo J 29:1637–1651.
Schlager MA, Serra-Marques A, Grigoriev I, Gumy LF, Esteves da Silva M, Wulf PS, Akhmanova A, Hoogenraad CC (2014) Bicaudal D family adaptor proteins control the velocity of Dynein-based movements. Cell Rep 8: 1248–1256.
Shafaq-Zadah M, et al. (2016) Persistent cell migration and adhesion rely on retrograde transport of β(1) integrin. Nat Cell Biol 18:54–64.
Solecki DJ, Govek EE, Tomoda T, Hatten ME (2006) Neuronal polarity in CNS development. Genes Dev 20:2639–2647.
Stenmark H (2009) Rab GTPases as coordinators of vesicle traffic. Nat Rev Mol Cell Biol 10:513–525.
Tahirovic S, Bradke F (2009) Neuronal polarity. Cold Spring Harb Perspect Biol 1:a001644.
Tao-Cheng JH (2020) Immunogold labeling of synaptic vesicle proteins in developing hippocampal neurons. Mol Brain 13:9.
Teoh JJ, Iwano T, Kunii M, Atik N, Avriyanti E, Yoshimura SI, Moriwaki K, Harada A (2017) BIG1 is required for the survival of deep layer neurons, neuronal polarity, and the formation of axonal tracts between the thalamus and neocortex in developing brain. PLoS One 12: e0175888.
Toriyama M, Shimada T, Kim KB, Mitsuba M, Nomura E, Katsuta K, Sakumura Y, Roepstorff P, Inagaki N (2006) Shootin1: a protein involved in the organization of an asymmetric signal for neuronal polarization. J Cell Biol 175:147–157.
Tronche F, Kellendonk C, Kretz O, Gass P, Anlag K, Orban PC, Bock R, Klein R, Schütz G (1999) Disruption of the glucocorticoid receptor gene in the nervous system results in reduced anxiety. Nat Genet 23:99–103.
Villarroel-Campos D, Bronfman FC, Gonzalez-Billault C (2016) Rab GTPase signaling in neurite outgrowth and axon specification. Cytoskeleton (Hoboken) 73:498–507.
Wang T, Liu Y, Xu XH, Deng CY, Wu KY, Zhu J, Fu XQ, He M, Luo ZG (2011) Lgl1 activation of rab10 promotes axonal membrane trafficking underlying neuronal polarization. Dev Cell 21:431–444.
Wanschers BF, van de Vorstenbosch R, Schlager MA, Splinter D, Akhmanova A, Hoogenraad CC, Wieringa B, Fransen JA (2007) A role for the Rab6B Bicaudal-D1 interaction in retrograde transport in neuronal cells. Exp Cell Res 313:3408–3420.
White J, et al. (1999) Rab6 coordinates a novel Golgi to ER retrograde transport pathway in live cells. J Cell Biol 147:743–760.
Yin DM, Huang YH, Zhu YB, Wang Y (2008) Both the establishment and maintenance of neuronal polarity require the activity of protein kinase D in the Golgi apparatus. J Neurosci 28:8832–8843.
Yonekawa Y, Harada A, Okada Y, Funakoshi T, Kanai Y, Takei Y, Terada S, Noda T, Hirokawa N (1998) Defect in synaptic vesicle precursor transport and neuronal cell death in KIF1A motor protein-deficient mice. J Cell Biol 141:431–441.
Yoshimi K, Kaneko T, Voigt B, Mashimo T (2014) Allele-specific genome editing and correction of disease-associated phenotypes in rats using the CRISPR-Cas platform. Nat Commun 5:4240.
Zahavi EE, Hummel JJA, Han Y, Bar C, Stucchi R, Altelaar M, Hoogenraad CC (2021) Combined kinesin-1 and kinesin-3 activity drives axonal trafficking of TrkB receptors in Rab6 carriers. Dev Cell 56:494–508.e497.
Zerial M, McBride H (2001) Rab proteins as membrane organizers. Nat Rev Mol Cell Biol 2:107–117.
Zhai RG, Vardinon-Friedman H, Cases-Langhoff C, Becker B, Gundelfinger ED, Ziv NE, Garner CC (2001) Assembling the presynaptic active zone: a characterization of an active one precursor vesicle. Neuron 29:131–143.
Zhao C, et al. (2001) Charcot-Marie-Tooth disease type 2A caused by mutation in a microtubule motor KIF1Bbeta. Cell 105:587–597.